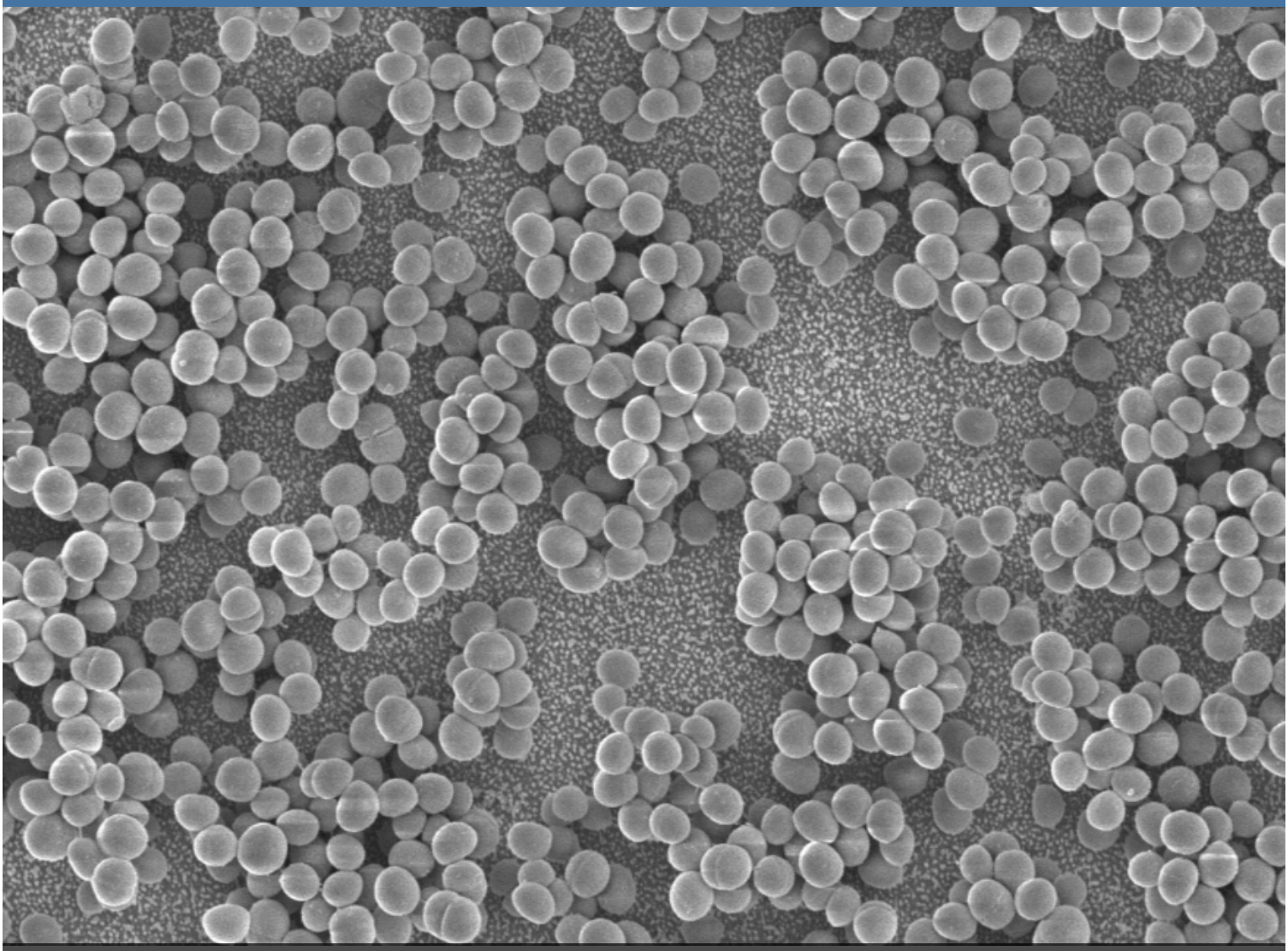

Interactions between Staphylococcus epidermidis, monocytes and nano structured gold surfaces

Magnus Forsberg

Master thesis in Medicine

Gothenburg 2013

The present thesis contains material (text, figures and tables) which has been published by Dove Medical Press (Svensson, S, Forsberg, M, Hulander, M, Vazirisani, F, Palmquist, Lausmaa, J, Thomsen, P and Trobos, M. Int J Nanomedicine).

In following parts have I done a large extent or all of the work: Surface preparation, Bacterial adhesion and biofilm formation on nanotopographic versus smooth surfaces, Bacterial strains and culturing, Live and dead fluorescence microplate readings, Viable counts, Monocyte co-culture experiments, Monocyte isolation, characterization and culture, Monocyte viability, Monocyte quantification, Monocyte gene expression and Monocyte cytokine secretion. For almost all other parts I have been of assistence to the other co-authors and therefore obtained insight in many different experimental texhniques and methods.

Interactions between *Staphylococcus epidermidis*, monocytes and nano structured gold surfaces

Master thesis in Medicine

Magnus Forsberg

Supervisors
Professor Peter Thomsen
Ph.D. Margarita Trobos

Institute of Clinical Sciences
Department of Biomaterials

UNIVERSITY OF GOTHENBURG

Programme in Medicine

Gothenburg, Sweden 2013

Table of Contents

Abstract

The role of material surface properties for the direct interaction with bacteria and the indirect route via host defense cells is not fully understood. Recently, nanostructured implant surfaces were suggested to possess antimicrobial properties. In the present study the adhesion and biofilm formation of *Staphylococcus epidermidis* and human monocyte adhesion and activation were studied separately and in co-culture in different in vitro models by using smooth (Au) and well defined nanostructured (AuNP) gold model surfaces. Two polystyrene surfaces were used as controls in the monocyte experiments. Fluorescent viability staining demonstrated a reduced viability of *S. epidermidis* close to the nanostructured surface, while the smooth Au correlated with more live biofilm. The results were supported by scanning electron microscopy observations, showing higher biofilm tower formations and more mature biofilms on Au compared to AuNP. Unstimulated monocytes on the different substrates demonstrated low activation as measured by chemiluminescence, gene expression of pro- and anti-inflammatory cytokines and cytokine secretion. In contrast, stimulation with opsonized zymosan or opsonized live *S. epidermidis* during 1 h, significantly increased the production of reactive oxygen species, the gene expression of tumor necrosis factor-alpha (TNF-α), interleukin-1beta (IL-1β), IL-6 and IL-10 and the secretion of TNF-α, demonstrating the ability of the cells to elicit a response and actively phagocytise the preys when present on all surfaces. In addition, cells on the smooth Au and AuNP showed a different adhesion pattern and a more rapid oxidative burst than on polystyrene upon stimulation. It is concluded that *S. epidermidis* decreased its viability initially when adhering to nanostructured compared to smooth gold surfaces, especially in the bacterial cell layers closest to the surface. On the other hand, material surface properties neither strongly promoted nor attenuated the activity of monocytes when exposed to zymosan particles or *S. epidermidis*.

Keywords: nanotopography, staphylococci, host defense, bacteria, zymosan, macrophage

Introduction

Biomaterial-associated infections (BAIs) are highly problematic for the patient, health care and society. The consequences of BAIs can be devastating and include potentially life-threatening systemic infections, tissue injury, device malfunction and ultimately a need to remove the implant (1, 2). Under normal conditions microorganisms that enter the body are kept under control by the immune system. The first lines of defense comprise a variety of factors, e.g. epithelial barriers, complement proteins, acute phase proteins and cytokines, and phagocytic cells such as monocytes, macrophages and neutrophils. However, when a foreign material is present, the host defense becomes hampered and it has been suggested that an "immuno-incompetent" zone is formed around the implant (3). In addition, adherent bacteria may form a biofilm that protects them from phagocytic uptake, bactericidal and opsonizing antibodies as well as antibiotic treatment (3). In such case, removal of the implant may be the only option in the attempt to eradicate the infection.

Staphylococcus species, especially *S. epidermidis* and *S. aureus*, are the predominant species found in BAIs, accounting for about 66% (1). Unfortunately, more and more bacteria acquire resistance against antibiotics (4), pushing further for preventive measures in order to reduce the infection rates.

Materials with nanotopographic features have been explored with respect to adhesion and function of various cell types, e.g. fibroblasts, osteoblasts, mesenchymal stem cells and keratinocytes (5-10). Less literature is available on the activities of inflammatory cells on defined, nanostructured surfaces (11-13), even though these cells are among the first to encounter an implanted device and have a decisive role in the acceptance of the implant. Nanostructured materials have also been suggested to play a role in bacterial adhesion. Bacteria have, in contrast to eukaryotic cells, a rigid cell wall with limited capability to deform upon attachment, implying that they do not react to structures smaller than themselves

(14). However, some studies do show a decrease in bacterial adhesion when exposed to nanotextured surfaces (15-17), but the results are contradictory and the contribution from surface chemistry cannot always be excluded (14).

In the present study we have investigated whether nanostructures 1) have an effect on bacterial adhesion and biofilm formation, and/or 2) have an influence on the behavior of immune cells in response to microbial stimuli. Selected for this purpose were very smooth gold sputtered silica wafers that can be modified with well-defined nanoparticles (35-40 nm) in a systematic manner using thiol-chemistry. These model surfaces possess the same chemical characteristics (18) and therefore enable a direct comparison of the role of surface nanotexture on the behavior of inflammatory cells and microorganisms. A strong biofilm-producing strain of *S. epidermidis* as well as primary monocytes isolated from human blood donors were used in the study. Zymosan, a cell wall product from *Saccharomyces cerevisiae*, was used as a non-living microbial control stimulus.

Material and methods

The material surfaces used in the study were a smooth Au surface (Au) and different nanostructured Au surfaces (AuND, AuNL, AuNP). Tissue culture plastic (TCP), the golden standard in cell culturing, and tissue culture treated Thermanox® plastic cover slips (Thx), that similar to the Au-surfaces can be transferred between wells, were used as control surfaces in the monocyte cell culture experiments.

Surface preparation

Synthesis of gold nanoparticles

Gold nanoparticles were prepared by reduction of HAuCl4 (Sigma-Aldrich) by sodium citrate (Sigma-Aldrich) using a modification of a previously described protocol (19). In brief, particles with an average size of 38 nm were synthesized by heating the $HAuCl_4$ (2.4 mM) solution to 60°C and adding 60°C tribasic sodium citrate solution (3.9 mM) (1:1). The synthesis was allowed for 1 h under stirring conditions. The particle stock solution was stored at 8°C until use.

Preparation of nanostructured gold surfaces

Gold sputtered silicon wafers (200 nm gold on a supporting layer of 10 nm of titanium) were purchased from Litcon AB, Sweden. The substrates were washed for 15 min at 80°C in basic piranha solution containing 3:1:1 MilliQ water, NH_3 (24%) and H_2O_2 (30%) and washed in excess of MilliQ water before incubation in 20 mM aqueous solution of cysteamine (Sigma-Aldrich) for 2 h. The surfaces were then rinsed with excess MilliQ water and incubated in the gold nanoparticle stock solution at room temperature overnight, resulting in nanostructured surfaces (AuNP). After incubation, surfaces were washed in excess of MilliQ water. Immediately before use, all surfaces (smooth and nanostructured) were cleaned in a

UV/ozone chamber for 15 min, washed in basic piranha for 10 min at 70°, rinsed with excess of water and finally blown dry in a gentle stream of N_2 (g).

In an initial subset of experiments, exclusively with *S. epidermidis* (live and dead fluorescence microplate readings), surfaces with high and low surface coverage of nanoparticles, Nano Dense (AuND) and Nano Light (AuNL), were prepared by controlling the electrostatic repulsion between the particles. The distance between colloids in an electrolyte depends primarily on the size of the electric double layer of counter ions surrounding the colloids. The inter-particle distance between gold nanoparticles suspended in an electrolyte can thus be controlled by changing the ionic strength of the electrolyte as described earlier (20, 21). Briefly, the gold nanoparticle stock solution was centrifuged at 1000g for 90 min and the pellet re-suspended in MilliQ-water or 10 mM sodium citrate (tri-basic) buffer at pH 4. Cysteamine functionalized gold substrates were then incubated in the nanoparticle solutions for 3 h and washed as described above prior to use.

Surface analysis

Surfaces were viewed in a Zeiss 982 Gemini digital scanning electron microscope (SEM, Oberkochen, Germany) in secondary electron mode, using the in-lens detector mode. Nanoparticle size and surface coverage (projected area) was calculated from SEM images through image analysis in the software ImageJ (National Institutes of Health, Bethesda, MD, USA); the images were thresholded to remove the background surface, and by assuming spherical particles, the average particle size and surface area coverage were calculated from pixel count. Additionally, surface roughness was evaluated using a Bruker Dimension 3100 atomic force microscope (AFM) with an nsc 15 tip (MicroMash) in tapping mode in ambient air. Water contact angles were measured on the experimental substrates to assess surface wettability and to confirm efficacy of the washing protocol. A 5 µl ultra-pure water droplet (MilliQ, 18.2MΩ) was applied on the surface and a side view image of the droplet was

captured with high magnification macro photography. Contact angles were then measured using the angle tool in ImageJ software.

Bacterial adhesion and biofilm formation on nanotopographic versus smooth surfaces

Bacterial strains and culturing

The biofilm producer strain *Staphylococcus epidermidis* ATCC 35984 obtained from the Culture Collection University of Göteborg (CCUG 31568) was used in this study. Single colonies from overnight cultures on Columbia horse blood agar plates (Media Department, Clinical Microbiology lab, Sahlgrenska University Hospital, Gothenburg, Sweden) were suspended in 4 mL RPMI 1640 medium containing GlutaMAX™ (Gibco) until OD (546 nm) of 0.25 (=10^8 CFU/mL). An inoculum suspension was prepared by diluting the OD suspension to 10^5 CFU/mL in pre-warmed RPMI medium. The RPMI medium was chosen since it was the most suitable medium to culture human monocytes and also supported the growth of *S. epidermidis*.

Live and dead fluorescence microplate readings

To examine the relative amount of adherent live and dead *S. epidermidis* after 24 h, an inoculum of 10^5 CFU/mL in RPMI medium was added to Au, AuND and AuNL surfaces (n = 3). After 24 h of static incubation at 37°C, the surfaces were carefully washed with 0.9% sterile saline (3×1 mL) and incubated with 250 µL of a pre-mixed staining solution from the FilmTracer™ LIVE/DEAD® Biofilm Viability kit (Invitrogen) for 30 min in dark. The kit provides a two-color fluorescence assay (SYTO® 9 and propidium iodide) of bacterial viability where all cells will be stained fluorescent green and cells with damaged membranes will be counter-stained and fluoresce red. The surfaces were then washed, transferred to black 24-well plates (lumox® multiwell, Sarstedt), and 500 µL saline was added to each surface. The microtitre plate was read by a FLUOstar Omega microplate reader (BMG Labtech,

Germany) for fluorescence, multichromatic, top optic reading, using excitation filter 485 nm and emission filter 520 nm. A scan matrix of 20x20 was used together with gains set to 1500 for SYTO9 and 2000 for PI fluorofores. Non-stained surfaces served as blanks. The experiment was repeated four times.

Viable counts

In order to test the initial adhesion and biofilm formation capacity of *S. epidermidis* on AuNP and Au the following static adhesion experiment was performed twice. An inoculum of 10^5 CFU/mL of *S. epidermidis* was prepared in RPMI medium and a total of 1 mL was added onto AuNP and smooth Au surfaces (n = 3). The surfaces and the bacterial suspension were incubated for 2 h, 24 h or 48 h at 37˚C under static conditions. After each time-point was reached, the surfaces were washed to remove non-adherent bacterial cells. The surfaces were transferred to new tubes containing 1 mL 0.9% saline + 0.1% triton-X, sonicated for 30 sec at 40 kHz and hard vortexed for 1 min in order to dislodge the adherent bacteria and break aggregates. SEM analysis of the surfaces afterwards showed a good detachment procedure with most of the surface area cleaned from bacteria. The sonicated suspension was assessed by quantitative cultures on blood agar plates. The number of colony-forming units (CFU) per surface was quantified by adding 0.1 mL of the sonicated suspension to serial dilutions until 10^{-6} in 0.9% saline + 0.1% triton-X. From the undiluted and the six dilutions CFU counting was performed (double measurements).

Scanning electron microscopy

Initial adherence and biofilm formation of *S. epidermidis* on AuNP and Au was assessed morphologically using SEM. Samples were washed with HBSS and fixated in 2% paraformaldehyde and 2.5% glutaraldehyde in 0.15 M sodium cacodylate buffer (pH 7.2) over night at 4°C. The samples were washed with 0.15 M sodium cacodylate buffer and post-fixated with 1% osmium tetroxide in 0.1 M sodium cacodylate buffer for 2 h at 4°C. Contrast

enhancement was performed with 1% thiocarbohydrazide for 10 min at room temperature followed by incubation in 1% osmium tetroxide in 0.1 M sodium cacodylate buffer for 1 h at 4°C. Dehydration was performed in a graded series of ethanol (70%-99.5%) and critical point drying by hexamethyldisilizane evaporation. The samples were mounted on stubs and sputtered with palladium before viewing in Zeiss 982 Gemini SEM operated at 3 kV.

Confocal laser scanning microscopy

To determine the capacity of *S. epidermidis* to form biofilm when growing onto AuNP and Au surfaces, 10^3-10^4 CFU/mL of *S. epidermidis* was incubated statically on the surfaces for 2 h, 24 h and 48 h. After each adhesion time-point the surfaces (n = 1) were carefully washed to remove non-adherent cells. A total of 200 µl of FilmTracer™ LIVE/DEAD® staining solution was added to the biofilms for 30 min at room temperature under dark conditions. Thereafter the surfaces were carefully washed and placed in 60 mm petri plates covered in saline for *in situ* visualization under the Confocal Microscope LSM710 (Carl Zeiss AB, water objective 20x/1.0). Gain settings for the 488 nm argon laser/561 nm DPSS laser at 2 h were set to 721/752, at 24 h to 519/691 and at 48 h to 400/691. Five different equidistant random spots (4 in the corners and 1 in the middle of the surface) were chosen to perform z-stacks every 3 µm. Three independent experiments were performed. Confocal biofilm images were analyzed using the COMSTAT2 (http://www.COMSTAT2.dk; Lyngby, Denmark) software that converts biofilm image stacks into three-dimensional outputs for quantitative analysis. The parameters analyzed were: biomass, maximum thickness and area occupied at the surface (z=0 µm) of live and dead cells (22). Biomass is how much of the image stack is covered by bacteria (live and dead); the maximum thickness represents the compacted thickness of the biofilm image stack; and the area occupied by bacteria in the layer closest to the surface is the area occupied by biomass (cells) in the first stack image (the substratum). The images were thresholded with a threshold of 30 for 2 h, 35 for 24 h and 40 for 48 h.

Monocyte co-culture experiments

Monocyte isolation, characterization and culture

Human monocytes were isolated from buffy coats obtained from six blood donors by using Ficoll separation followed by negative selection on a magnetic column (MACS, Miltenyi Biotec); viability 98.7±1.9%. For characterization, samples of 500.000 cells were stained with CD14-PE and CD45-FITC antibodies and analyzed using flow cytometry (BD FACSCalibur™, BD Biosciences), and the monocyte purity was estimated to 85.4±4.7%. The cells were seeded on nanostructured (AuNP) or smooth (Au) gold squares (8×8 mm), on cell culture treated Thermanox® (Thx) plastic coverslips (diameter 13 mm; Nunc™, Thermo Scientific, Denmark), and on tissue culture treated polystyrene (TCP) in 24- or 48-well plates (Falcon™, BD Biosciences, Bedford, MA, USA or Nunc™, Thermo Scientific, Denmark) to best fit the size of the different materials. The experimental procedure is outlined in Figure 1. One million cells in 1 mL RPMI medium supplemented with 5% fetal bovine serum were seeded in all wells and cultured in humidified air with 5% CO_2 at 37°C. Monocytes were allowed to adhere to the surfaces for 18 h, after which the medium was removed, the surfaces were transferred to new wells and 1 mL fresh medium was added. After further 24 h culture, the cells were divided into three groups: 1) unstimulated cells, 2) zymosan-stimulated cells, or 3) *S. epidermidis*-stimulated cells. Monocytes were stimulated by adding serum-opsonized zymosan A particles (final concentration 2×10^7 particles/mL; Sigma-Aldrich) or serum-opsonized *S. epidermidis* (final concentration 10^8 CFU/mL) for 1 h, corresponding to a particle-to-cell ratio of 20 particles and 10^2 bacterial cells, respectively, per seeded monocyte. Zymosan was opsonized in active human serum in phosphate buffer solution (PBS) (1:1) for 1 h at 37°C. From an overnight culture of *S. epidermidis* on blood agar, a colony was inoculated in Tryptic Soy Broth (TSB) and incubated at 37°C for 4 h under shaking (150 rpm) until exponential growth (in duplicate), and opsonized in 10% active human serum in Hank's

Buffered Salt Solution (HBSS) for 5 min at 37°C. Triplicate or duplicate samples were used for all analyses and six independent experiments were performed.

Figure 1: Scheme for co-culture experiments.

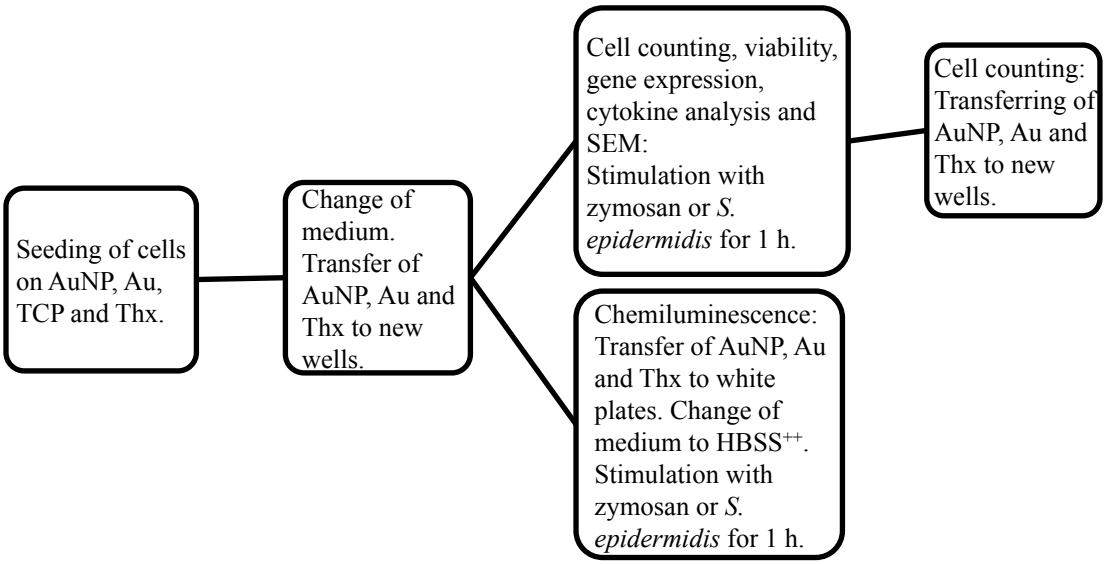

Monocyte viability

Cell viability was assessed by using the centrifuged cell medium for evaluation of lactate dehydrogenase (LDH) content (C-laboratory, Sahlgrenska University Hospital, Göteborg, Sweden). LDH is a marker of cell membrane injury that can be measured using a spectrophotometric evaluation of LDH-mediated conversion of lactate to pyruvate. The detection limit of the instrument was 0.17 µkatal/L. Values below the detection limit were set to 0.16 µkatal/L.

Monocyte quantification

Adhesion of monocytes on AuNP, Au, TCP and Thx was assessed 1) after 18 h and 2) after the 1 h stimulation period to compare cell adhesion of unstimulated, zymosan-stimulated, and *S. epidermidis*-stimulated samples. Cells in the supernatant and on the plastic (TCP) below the materials in the well were also counted separately. Quantification of cells was performed by using the Nucleocounter®-system (ChemoMetec A/S, Denmark). The samples were

treated with lysis buffer and stabilization buffer. Lysed samples were loaded in a Nucleocassette™ precoated with fluorescent propidium iodide that stains the cell nuclei and then quantified in the NucleoCounter®.

Scanning electron microscopy

Adherent monocytes with and without stimulation of zymosan or *S. epidermidis* on AuNP, Au and Thx were fixated and prepared as described previously. The surfaces were visualized by using a mixture of secondary and backscattered electrons in a Zeiss 982 Gemini SEM operated at 3 kV.

Quantitative RT-PCR

RNA was extracted from 137 samples in total, resulting in n = 8-15 for each group. Cells on AuNP, Au, TCP and Thx were lysed in 200 µL RLT lysis buffer (Qiagen, Germany) and frozen at -80°C prior to total RNA extraction using the NucleoSpin® RNA XS kit (Macherey-Nagel, Germany), as described in the manufacturer's instructions. The RNA quality and concentration were determined for selected samples using an Agilent 2100 Bioanalyzer (Agilent Technologies, Foster City, CA, USA) for pico profile, and a nanospectrophotometer (IMPLEN NanoPhotometer™ Pearl, Germany).

Total RNA was converted to cDNA by using TATAA GrandScript cDNA Synthesis Kit (TATAA Biocenter AB, Sweden) in 10 µL reactions. The samples were diluted 15X and real-time RT-PCR analysis was performed in duplicates in 10 µL reactions on the QuantStudio 12K Flex platform (Life Technologies) using TATAA SYBR® GrandMaster Mix (TATAA Biocenter AB) and primers (final conc. 400 nM) for 10 target genes and two reference genes. The genes of interest were coding for interleukin 1beta (IL-1β), IL-6, IL-10, tumor necrosis factor alfa (TNF-α), integrin β1 (CD29), integrin β2 (CD18), integrin αv (CD51), integrin αm (CD11b), superoxide dismutase 2 (SOD2) and Nox2 (cytochrome b-245). Peptidylprolyl isomerase A (PPIA) and ribosomal protein large P0 (RPLP) was identified as the best

reference genes in the TATAA reference gene panel based on analysis in GenEx software (MultiD Analyses AB, Sweden) using the NormFinder and the geNorm algorithms. Raw data was analyzed in QuantStudio 12K Flex Software 1.1.2 (Life Technologies) and processed in GenEx using the relative comparative Cq method.

Cytokine determination

After centrifugation of medium from cells cultured on AuNP, Au, TCP and Thx surfaces with or without zymosan or *S. epidermidis,* the supernatant was analyzed with respect to IL-1β, IL-6, IL-10 and TNF-α using commercial ELISA kits (Quantikine®, R&D Systems) according to the manufacturer's instructions. The detection limits are less than 1 pg/mL, 0.7 pg/mL, 3.9 pg/mL and 5.5 pg/mL, respectively. The optical density was measured with a microplate reader and translated to cytokine levels using the accompanied software.

Reactive oxygen species measured by luminol-mediated chemiluminescence

Monocytes/Macrophages cultured on AuNP, Au, TCP and Thx (n = 2-3) were evaluated for their ability to produce reactive oxygen species (ROS) upon stimulation with zymosan or *S. epidermidis*. The surfaces were transferred to white 24-well plates (Visiplate™ TC, PerkinElmer, USA) and $HBSS^{++}$ (with Ca^{2+} and Mg^{2+}) with zymosan or *S. epidermidis* stimulus was added to a final volume of 1.96 mL before insertion into a microplate reader (37°C) equipped with luminescence optics and a 3 mm light guide for increased sensitivity (gain 4000). A kinetic program was run for 80-90 cycles (1 min per cycle) where light emission from each well was measured every minute. In the fifth cycle, 40 µL of luminol was automatically injected (final concentration of 5×10^{-5} M; Fluka/Sigma-Aldrich (Cat No 09253), Germany) followed by 5 seconds of shaking, for detection of reactive oxygen species formed in the samples. Non-stimulated samples were used as controls (n = 2). Upon termination of the experiment the cells were quantified. One well without seeded cells, but with HBSS and luminol, was used as a blank. The obtained data points were divided by the

total cell number in each well and the values were analyzed in MATLAB®, software version R2011a (MathWorks, Inc., MA, USA) where graphs were created using the Smoothing Spline-method (smoothing parameter 0.001). The curve for each sample was then analyzed for total chemiluminescence (CL) produced (integral under the curve), peak CL and time to peak CL, for x-values between 3 and 80 min.

Focused ion beam scanning electron microscopy

Samples prepared for morphological observations of interactions between monocytes/macrophages and zymosan and *S. epidermidis*, respectively, were analyzed in a dual beam focused ion beam (FIB) system (Strata DB 235, FEI, The Netherlands) operated at 30.0 kV. When interesting cells were localized, a protecting layer of platinum was sputtered over the cell surface and cross sections of the cells were exposed by FIB-milling and then imaged by SEM.

Statistics

All results are presented as mean ± standard deviation. The data was statistically evaluated by one-way analysis of variance (ANOVA) followed by Tukey's post hoc test or independent sample t-test (2-tailed) using 95% confidence interval in PASW/Statistics 18.0 (SPSS Inc., Chicago, USA) or SPSS version 21 (IBM Corp., Armonk, NY, USA). Evaluation of gene expression data was based on the logarithmic Cq-values. Statistical differences in the graphs and tables are denoted by letters, where values/bars in the same table/graph that share the same letters are significantly different ($P < 0.05$).

Results

Materials

Material characterization

Physicochemical properties of the experimental surfaces are summarized in Figure 2. Surface roughness was increased on the smooth gold substrates from 0.9 to 32 nm (rms) by the immobilized nanoparticles (AuNP). On TCP and Thx the roughness was expectedly low (1.9 nm rms). Au, TCP and Thx had water contact angles in the same range, while AuNP demonstrated a considerably more hydrophilic surface. The lower contact angle on nanostructured surfaces is in accordance with Wenzel's theory of increased wetting on nanostructured hydrophilic surfaces.(23) Average particle size and surface coverage of the AuNP surface was 31±6 nm and 38±4% respectively. On the AuND and AuNL surfaces the average particle size was 39±2 nm and the particle surface coverage 28% and 17%.

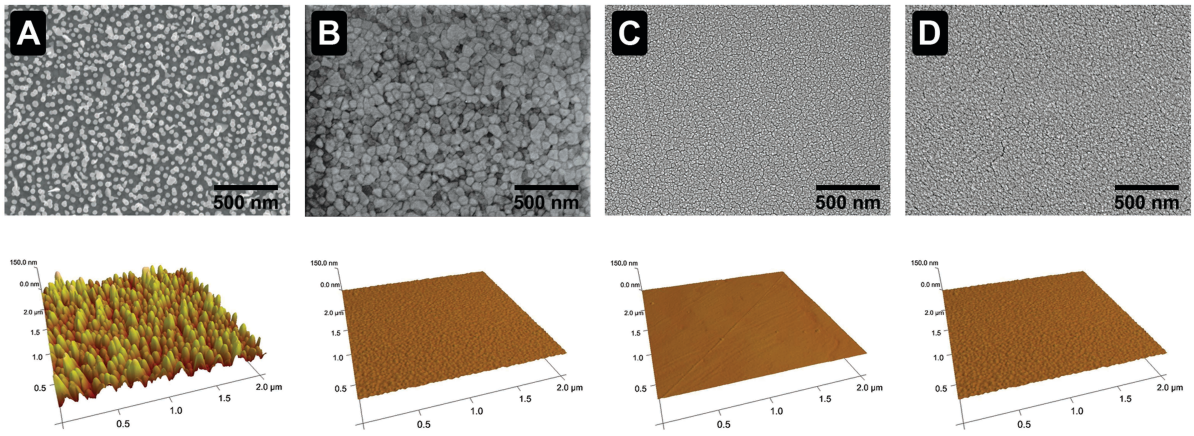

	AuNP	Au	TCP	Thx
Ra (nm)	26	0.7	1.5	1.5
Rms (nm)	32	0.9	1.9	1.9
Particle surface coverage (%)	31 *(±6)*	-	-	-
Average particle size (nm)	38 *(±4)*	-	-	-
Water contact angle (degrees)	24 *(±11)*	48 *(±12)*	59 *(±2)*	61 *(±3)*

Figure 2: Material characterization of AuNP (A), Au (B), TCP (C) and Thx (D). Top panel: SEM. Middle panel: AFM. Bottom panel: Physicochemical properties

Bacterial adhesion and biofilm formation on nanotopographic versus smooth surfaces

Live and dead fluorescence microplate readings

After 24 h incubation, significantly more live bacteria (Figure 3) were detected on smooth Au surfaces compared to AuNL and AuND. No differences were seen in the amount of dead bacteria.

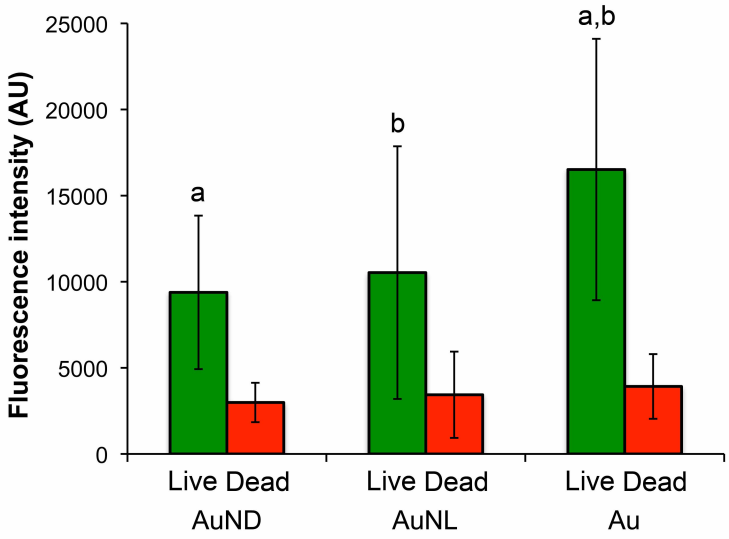

Figure 3: Live and dead fluorescence staining of adherent *Staphylococcus epidermidis* on AuNP and Au after 24h static incubation in RPMI-medium. Data represents mean ± standard deviation (n = 12). Significant differences between surfaces are indicated by letters ($P < 0.05$).

Viable counts

Similar amounts of viable *S. epidermidis* adhered to both AuNP and Au surfaces when recovered after 2, 24 and 48 h (Figure 4). The major increase in viable numbers occurred during the period from 2 to 24 h, when the formation of the biofilm and accumulation phase commonly take place. From 24 h to 48 h there was a small increase in viable numbers on both surfaces; this may be due to a lack of nutrients (no change of media) and/or dispersal events from the biofilm.

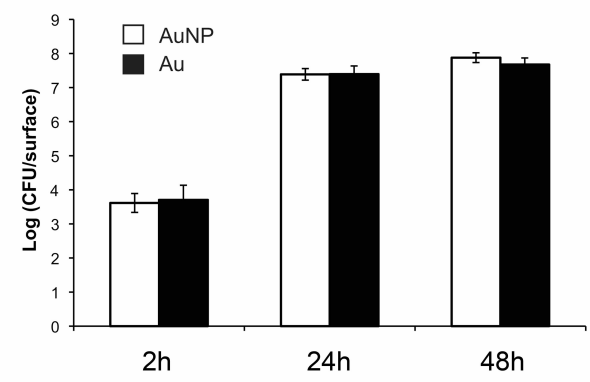

Figure 4: Viable counts of adherent *Staphylococcus epidermidis* on AuNP and Au after 2, 24 and 48 h of static incubation in RPMI medium. Data represents mean ± standard deviation (n = 6).

Scanning electron microscopy

SEM analysis of *S. epidermidis* on AuNP and Au revealed very few attached cells after 2 h on both surfaces. After 24 and 48 h the amount of bacteria had increased considerably and a general impression was that bacterial cells on smooth Au had an earlier onset of biofilm formation compared to AuNP. After 24 h the bacterial cells on smooth Au displayed intercellular slime connecting biofilm, while this was observed on AuNP after 48 h (Fig. 5). In addition, more mature biofilms with higher tower formations were observed on Au compared to AuNP after 48 h (Figure. 5).

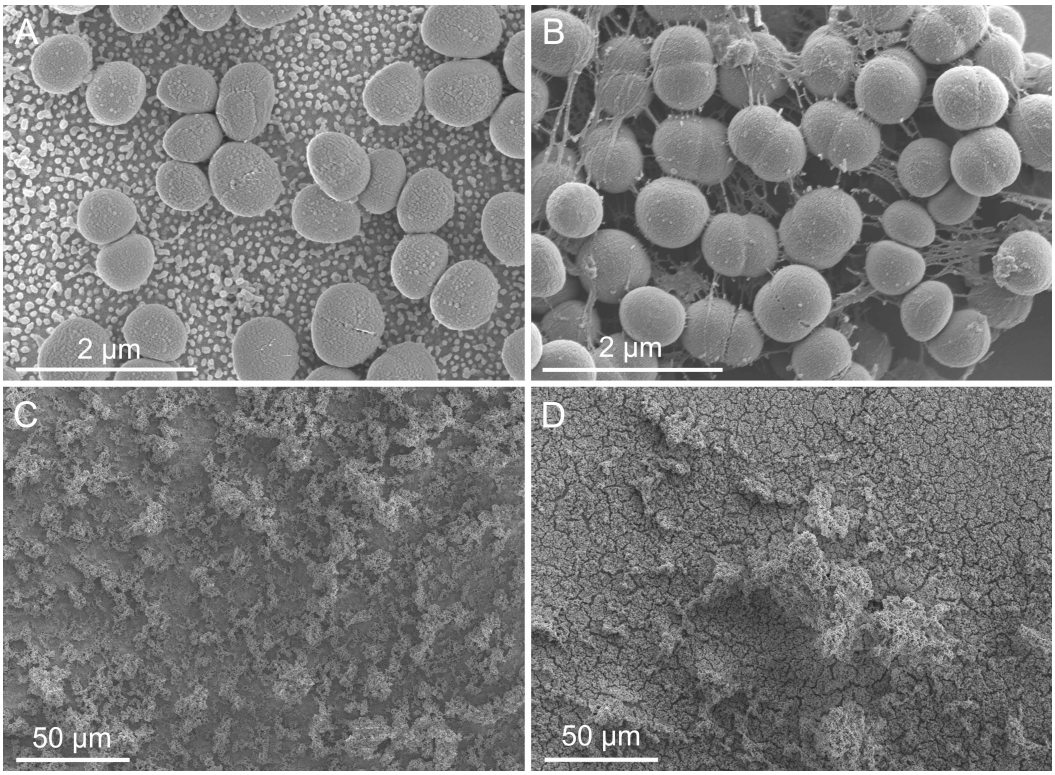

Figure 5: *Staphylococcus epidermidis* adherent on AuNP and Au after 24 and 48 h as visualized with SEM. After 24 h *S. epidermidis* on smooth Au surfaces (B) displayed more cell-connecting slime compared to nanostructured Au (A). A mature biofilm with high tower formations was seen on smooth surfaces (D) after 48 h, while the bacteria on nanostructured Au (C) were more horizontally scattered.

Confocal laser scanning microscopy

Figure 6 shows the results of the analysis of the confocal laser scanning microscopy (CLSM) images taken from biofilms. After 2 h of static adhesion of *S. epidermidis* to Au and AuNP surfaces, significantly more amount of dead biomass was found on nanostructured surfaces compared to smooth.

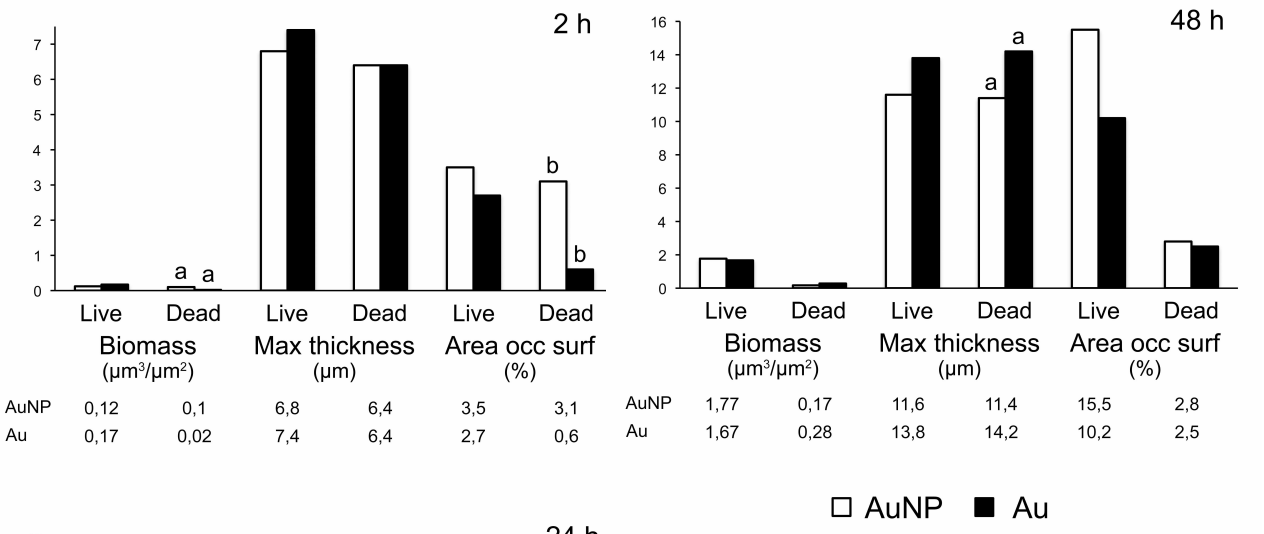

Figure 6:
CLSM analysis of *Staphylococcus epidermidis* biofilms grown on Au and AuNP surfaces for 2, 24 and 48 h under static incubation in RPMI medium. The total biomass, the maximum thickness of the biofilm and the area occupied at the surface by live and dead cells were analyzed by COMSTAT2 software.
Data represents mean (n = 3). Significant differences between surfaces are indicated by letters ($P < 0.05$).

Furthermore, the area occupied by dead cells in close contact to the surface was likewise greater on nanostructured than on smooth surfaces. Additionally, after 24 h of biofilm formation the area occupied by dead cells on nanostructured surfaces was also significantly greater (Figure 7).

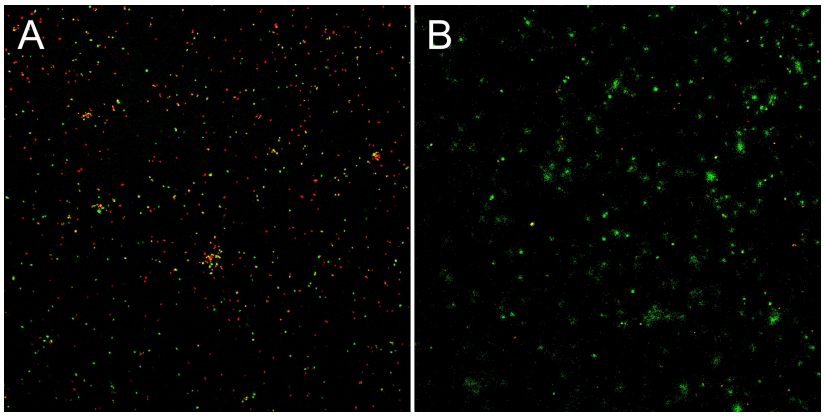

Figure 7: Live and dead fluorescence staining of *S. epidermidis* at the surface interface (z=0-3 µm) on AuNP (A) and Au (B) surfaces after 24 h of static incubation in RPMI medium as analyzed by CLSM. Green indicates live cells; red indicates dead cells.

Overall, thicker biofilms of both live and dead cells were formed on smooth compared to nanostructured surfaces after 24 h and 48 h.

Monocyte co-culture experiments

Monocyte viability

The cell viability, as measured by LDH, was high on all materials, irrespective of zymosan- or *S. epidermidis*-stimulation, with average values between 0.2 and 0.4 µkatal/L.

Monocyte adhesion

Significantly more cells attached to TCP compared to all other materials, while Thx had significantly less adherent cells compared to all other materials (Figure 8). Interestingly, upon stimulation the adhesion pattern differed between the materials: cell attachment increased on TCP, while it decreased on both AuNP and Au when compared to non-challenged cells (Figure 8).

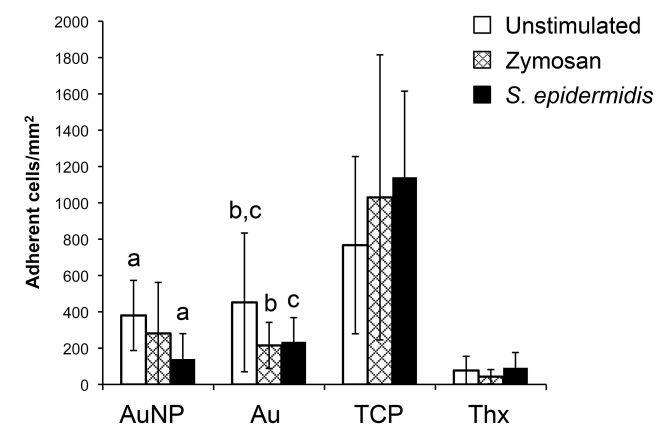

Figure 8: Number of adherent monocytes per mm^2 on AuNP, Au, TCP and Thx after 18 h primary adhesion followed by 24 h culture and 1 h challenge with either opsonized zymosan particles or opsonized *Staphylococcus epidermidis*. Unstimulated cells were used as control. Data represents mean ± standard deviation (n = 11-15). Significant differences between treatments are indicated by letters ($P < 0.05$).

Despite these differences in adherent cells, the number of supernatant cells increased with zymosan- and even more with *S. epidermidis* stimulation for all materials.

Adherent cells on AuNP, Au and Thx were viewed in SEM with and without addition of stimuli (Figure 9).

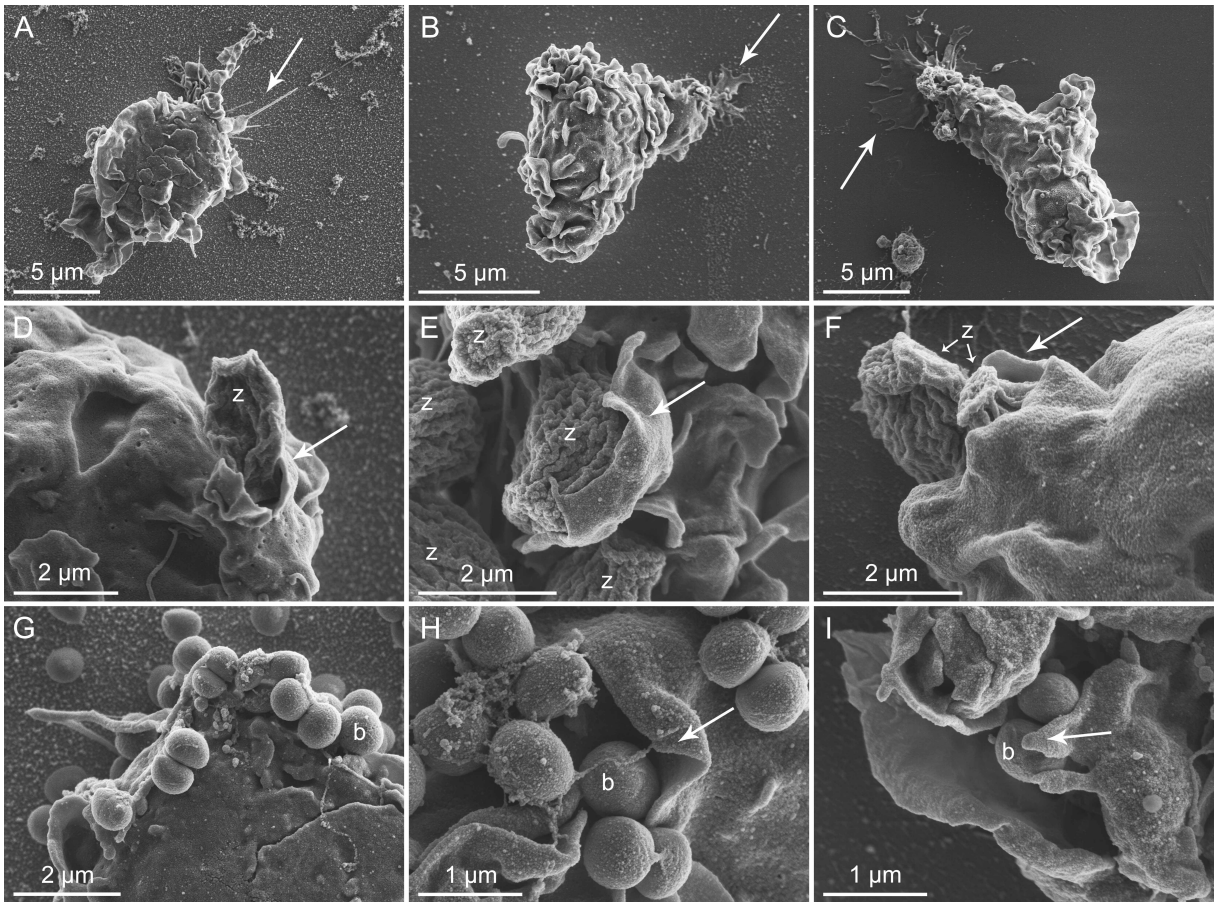

Figure 9: Monocytes on AuNP (A), Au (B) and Thx (C) surfaces in general demonstrated a rounded morphology with a moderate number of membrane ruffles/ridges with non-preferential directions. The cell-material surface interaction was morphologically evident in areas with cytoplasmic extensions, either being in the form of distinct, thin, spikes of variable length (arrow in A) or as thin, spread extensions (arrows in B and C). Cells with a polarized morphology were also observed (examples in B and C), suggestive of being in the process of attachment, detachment or migration. Details of monocyte-zymosan particle interactions are observed morphologically in D-F. Typically, oval shaped zymosan particles having finely, undulating ridges were clearly distinguishable. Several zymosan (z) particles were enveloped by pseudopods (arrows). A large number of *S. epidermidis* (being 0.5-1 µm round shaped cocci) were detected in close association with the monocyte membrane (G-I). Multiple bacteria (some of which are denoted b) were clustered and enveloped by large, thin-walled pseudopods (arrows) in an apparent phagocytic process. **Notes:** z indicates zymosan particles; b indicates bacteria (*S. epidermidis*)

The cells had a lot of contacts with the different preys, sometimes with extending filopodia reaching out for the preys. Many preys were also attached directly to the cell body-membrane and some of these were half way phagocytised into the monocyte/macrophage. A general

impression was that the cell-surface attachment tended to be more filopodia-dependent on the AuNP surfaces, while cells on the smooth Au and Thx surfaces had a much larger part of the plasma membrane in close contact with the surface. In addition, presumingly dead cells (apoptotic bodies) were seen free on the surface and in the process of being phagocytised by cells on all surfaces. Induction of apoptosis in monocytes/macrophages is normal in *in vitro* environments (24) and the process per se is crucial for proper maintenance of the immune system.

Monocyte gene expression

To explore whether the different material surfaces induced different gene expression, a panel of four cytokines was used (Figure 10). When comparing the different materials during unstimulated conditions, Thx showed significantly higher expression of TNF-α and IL-1β. However, AuNP did not induce a different response. After a 1 h stimulation period with either zymosan or *S. epidermidis* no differences were noted in the gene expression between any of the surfaces. Nevertheless, the stimulation provoked a significant increase of the pro-inflammatory cytokines TNF-α, IL-1β and IL-6 upon stimulation with both zymosan and *S. epidermidis*, with higher levels for cells stimulated with *S. epidermidis*, on all materials. The anti-inflammatory IL-10 was significantly higher for *S. epidermidis*-stimulated samples on all materials, but not for zymosan. The data on gene expression of SOD2 and Nox2, relevant for cell oxidative metabolism, is found in Figure 11.

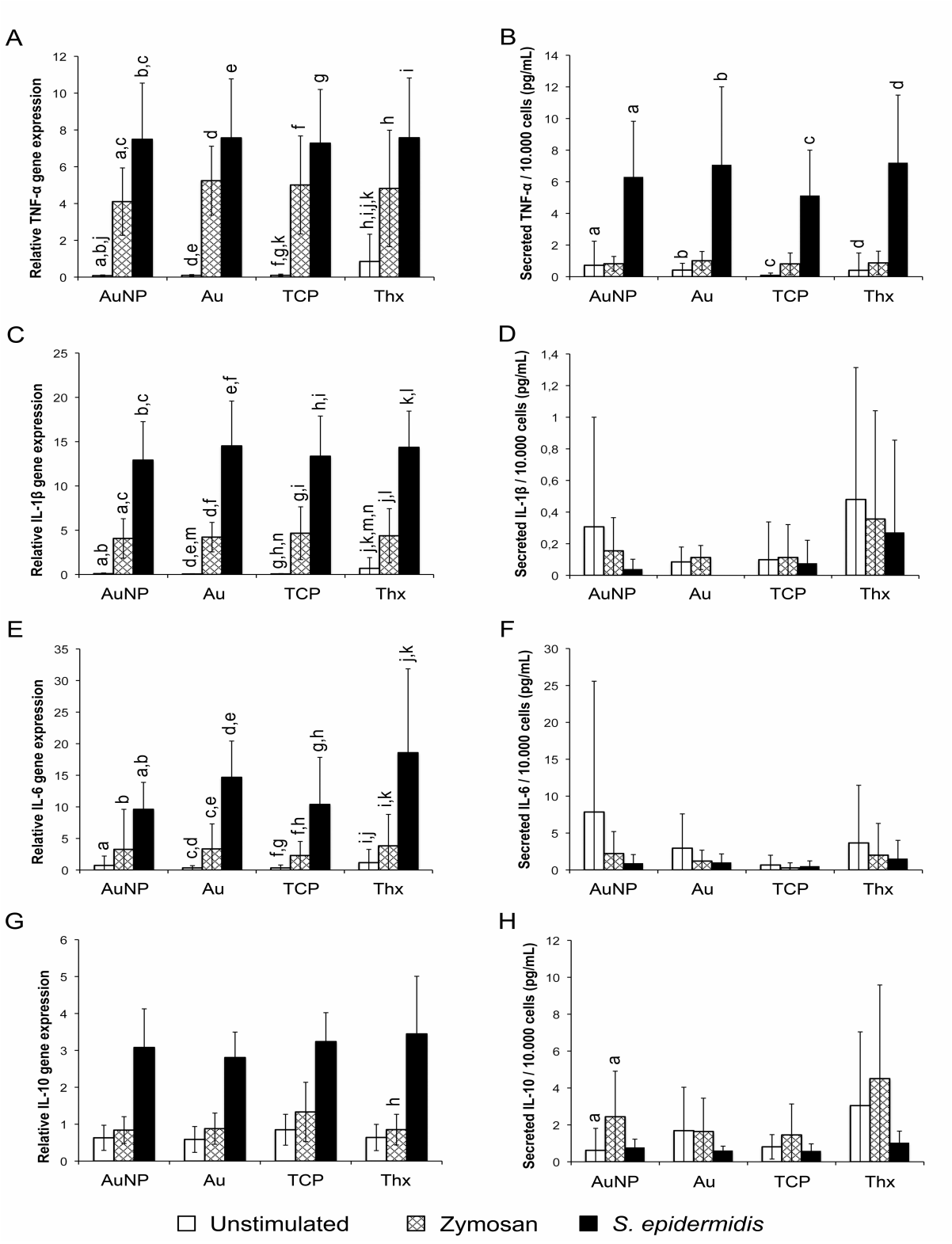

Figure 10. Gene expression (left panel) and cytokine secretion (right panel) of pro- and anti-inflammatory cytokines from monocytes on AuNP, Au, TCP and Thx. Gene expression of TNF-α (A), IL-1β (C), IL-6 (E) and IL-10 (G) was analyzed from adherent cells after 1 h stimulation with either opsonized zymosan particles or opsonized *Staphylococcus epidermidis*. Secretion of TNF-α (B), IL-1β (D), IL-6 (F) and IL-10 (H) proteins is presented as amount of cytokines per 10.000 total cells. Unstimulated cells were used as control.
Data represents mean ± standard deviation (n = 8-15 and n = 11-18 for gene expression and protein data, respectively). Significant differences between stimulus or material surfaces are indicated by letters ($P < 0.05$).

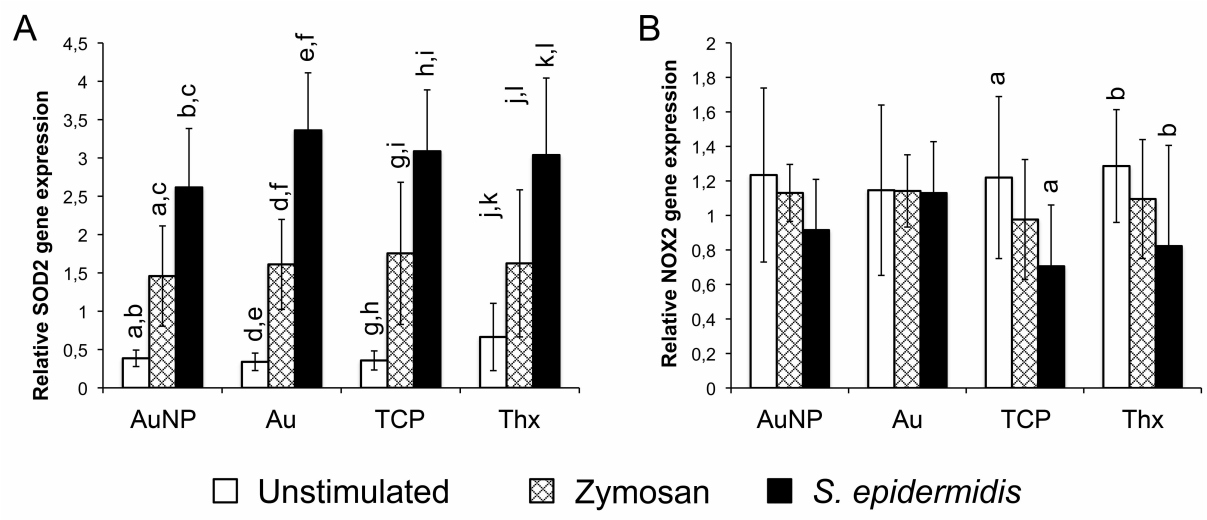

Figure 11. Gene expression of oxidative burst-related enzymes SOD2 (A) and Nox2 (B) in adherent monocytes on AuNP, Au, TCP and Thx after 1 h stimulation with either opsonized zymosan particles or opsonized *Staphylococcus epidermidis*. Unstimulated cells were used as control.
Data represents mean ± standard deviation (n = 8-15). Significant differences between stimulus or material surfaces are indicated by letters ($P < 0.05$).

Unstimulated cells showed a significantly higher expression on Thx. This difference was however leveled out upon stimulation when the expression was significantly induced, both for zymosan and even more for *S. epidermidis*. Nox2 was, on the other hand, relatively stable for AuNP and Au, while a significant decrease in expression was noted for TCP and Thx when stimulated with *S. epidermidis*.

Four different cell adhesion markers were analysed: integrin β1 (CD29), integrin β2 (CD18), integrin αv (CD51) and integrin αM (CD11b). Heterodimers of integrin β2 and integrin αM constitute the complement receptor 3 (CR3) which is implicated e.g. in the phagocytosis of serum opsonized microbes. However, gene expression data revealed a decrease in the expression of the CR3 subunits upon stimulation, with significant differences between 12). No significant differences were found for integrin β1 and integrin αv. unstimulated and *S. epidermidis*-stimulated samples for integrin β2 on all surfaces (Figure 12.)

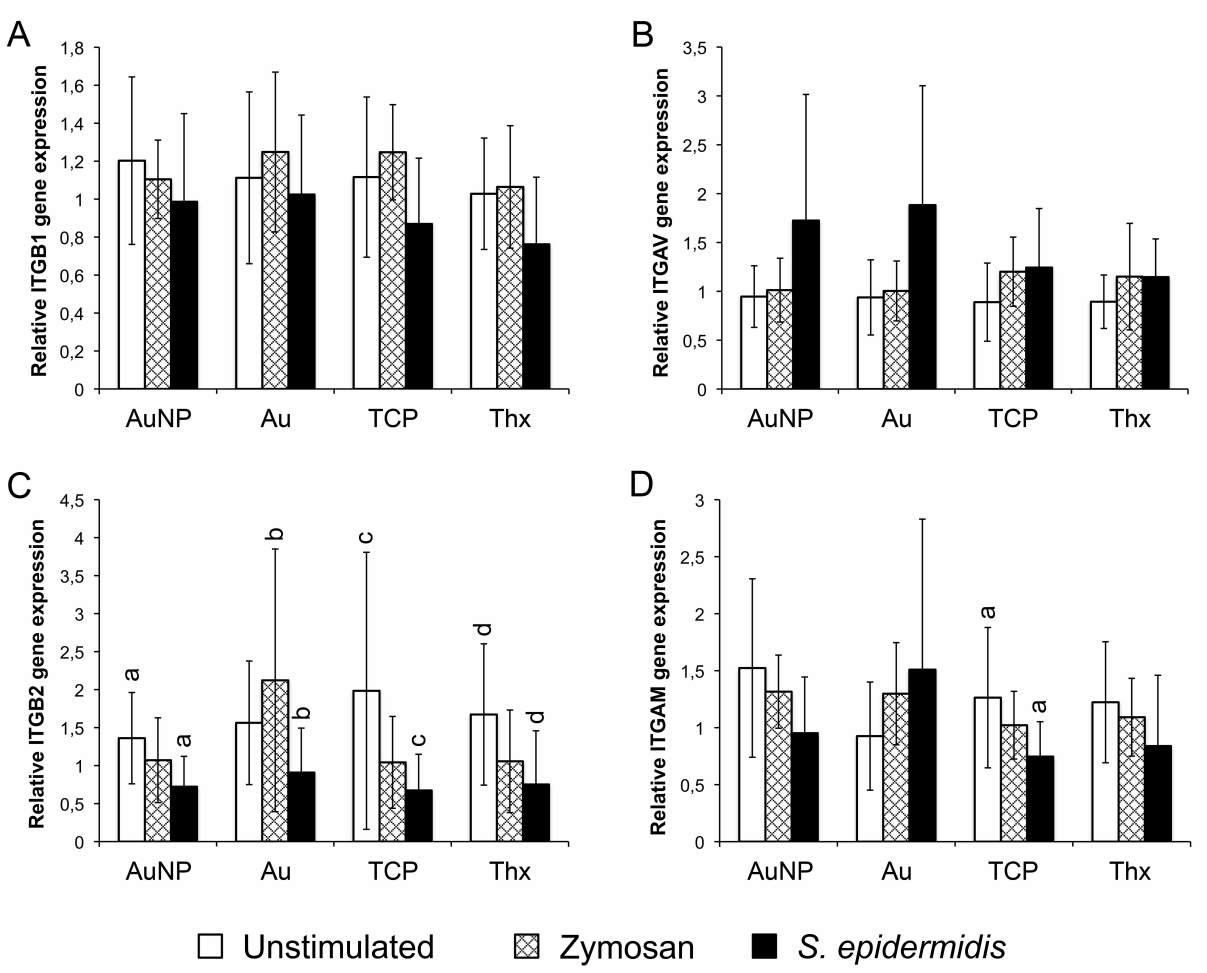

Figure 12. Gene expression of integrin β1 (A), integrin αv (B), integrin β2 (C) and integrin αM (D) in adherent monocytes on AuNP, Au, TCP and Thx after 1 h stimulation with either opsonized zymosan particles or opsonized *Staphylococcus epidermidis*. Unstimulated cells were used as control.
Data represents mean ± standard deviation (n = 8-15). Significant differences between stimulus or material surfaces are indicated by letters ($P < 0.05$).

Monocyte cytokine secretion

Cytokines detected in the supernatants of stimulated or unstimulated cells on different material surfaces are shown in Figure 10. Cells on all surfaces were induced to secrete significantly more TNF-α upon *S. epidermidis* stimulation. Zymosan also induced a small TNF-α increase, although not significantly different to unstimulated samples. A more pronounced production of IL-10 was noted for zymosan stimulated samples on AuNP. However, the amounts of IL-1β and IL-6 were similar for all surfaces and stimuli.

Monocyte oxidative response and phagocytosis

Stimulation of the cells with opsonized zymosan particles or opsonized *S. epidermidis* resulted in a significant increase in ROS production (Figure 13), while the unstimulated cells had CL production in the same level as the HBSS blanks. The amount of CL produced showed to be linearly dependent on the number of cells, allowing for the use of CL per cell when comparing activity on different materials. Also, opsonization of zymosan and *S. epidermidis* caused a higher oxidative response than the use of non-opsonized preys (data not shown). Interestingly, cells challenged with zymosan always gave a significantly higher response than cells challenged with *S. epidermidis*, (both total ROS response and peak ROS) (Figure 13, Table 1).

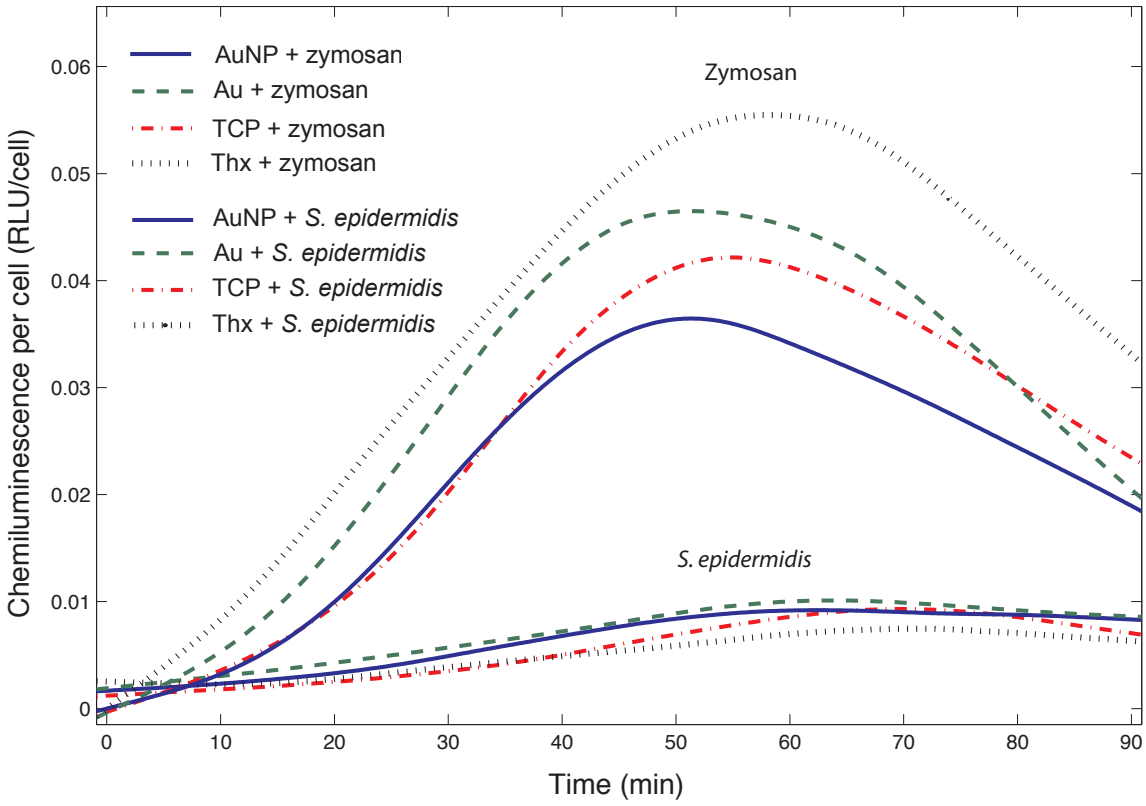

Figure 13. Representative graph of monocyte ROS production on AuNP, Au, TCP and Thx in response to opsonized zymosan particles and opsonized *Staphylococcus epidermidis* as measured by CL.

Table 1. Production of reactive oxygen species (as measured by chemiluminescence) in monocytes cultured on AuNP, Au, TCP and Thx surfaces in response to opsonized zymosan particles or opsonized *Staphylococcus epidermidis.*

	Zymosan			***S. epidermidis***		
	Total ROS (RLU/cell, 10^{-2})	*Peak ROS (RLU/cell, 10^{-3})*	*Time to peak (min)*	*Total ROS (RLU/cell, 10^{-2})*	*Peak ROS (RLU/cell, 10^{-3})*	*Time to peak (min)*
AuNP	205±59[a]	44±14[b]	56.7±6.2[c]	49±24[e]	10±4[h]	60.2±7.7[k]
Au	226±62	48±14	55.7±6.0[d]	45±18[f]	9±3[i]	54.0±11.5[l,m]
TCP	224±90	47±18	59.5±6.6	74±46 [e,f,g]	16±7 [h,I,j]	69.5±11.1[k,l]
Thx	266±84[a]	57±20[b]	62.5±8.7[c,d]	47±29[g]	10±5[j]	67.1±9.6[m]

Significant differences between material surfaces are indicated by letter superscripts ($P < 0.05$).

The amount of total ROS response per cell (integral under the curve) differed between materials and preys (Table 1). Cells on Thx had the highest activity when stimulated with zymosan, while cells on TCP had the highest activity when stimulated with *S. epidermidis*. The time to peak was not consistent between the different stimuli, but was always faster for the two Au-surfaces compared to the two plastic surfaces.

Increased ROS levels indicate interaction between the cells and zymosan/*S. epidermidis*, but to prove internalization of the preys the FIB-technique was employed. Although the cells did not always have visible contact with the preys on the cell surface, a cut through the cell revealed internalized particles and bacteria in the cell interior, irrespective of the surface used (Figure 14). *S. epidermidis* was clearly seen as small compact round cocci, while the zymosan was more structured and harder to discern. Unstimulated cells did not reveal similar structures in the cell interior.

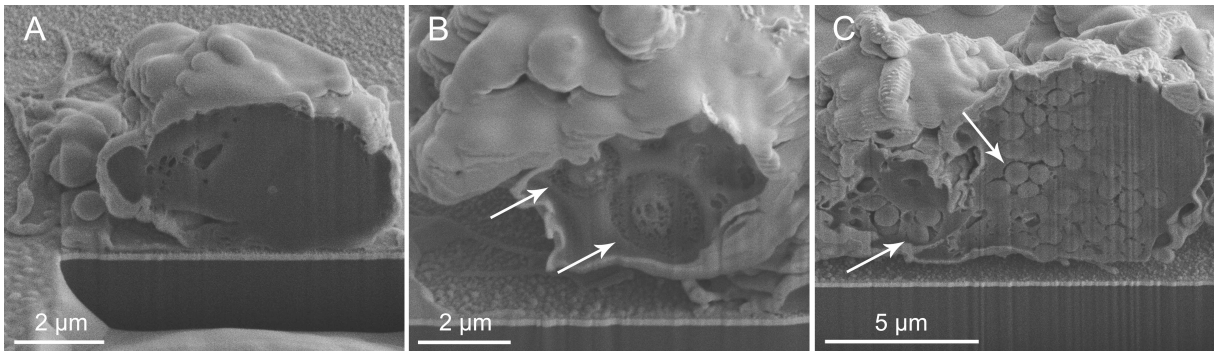

Figure 14. Phagocytosis of opsonized zymosan particles and opsonized *Staphylococcus epidermidis* by monocytes. Internalization of zymosan particles (B) and *S. epidermidis* (C) was evident on all surfaces, exemplified here by monocytes on AuNP, after 1 h of stimulation. Unstimulated monocytes lacked presence of internal preys (A). The cell surface was protected by a thin platinum film before ion milling of the cell in a FIB-SEM. Zymosan (B) and *S. epidermidis* (C), some of which are marked by arrows, are internalized by monocytes.

Discussion

There are at least two possible mechanisms by which material surfaces can reduce the incidence of medical device-related infections. Firstly, the material surface may have direct effects on the microorganisms. Secondly, the surface may have indirect effects on microorganisms by promoting antimicrobial host defense mechanisms. In an *in vivo* situation, both of these components are likely to be present, as well as proteins and other cell types. In the present study we tried to model these events *in vitro* by exploring the behaviour of bacteria and monocytes/macrophages separately as well as in combination. We have chosen to evaluate one specific type of nanofeatures, i.e. 35-40 nm sized Au particles immobilised on smooth Au surfaces, and compare it to its smooth counterpart. Previous studies have shown that these surfaces have identical surface chemistry (18), thus ensuring that any influence on the bacteria or monocytes derives solely from the changes in surface nanotopography.

Surface nanotopography influences bacterial adhesion and biofilm formation

The results of live/dead fluorescence plate readings demonstrated that the total number of live cells was significantly lower on the nanostructured Au-surfaces (AuND and AuNL) compared to the smooth Au control surfaces after 24 h adhesion. This also correlated with the results obtained from CLSM where the live/dead cell biomass ratio was 9x higher at the substrate interface (2 h) on smooth surfaces compared to nanostructured. This is in accordance with previous observations of decreased biofilm formation and bacterial adhesion on nanostructured substrates. (17, 25, 26)

For a given surface chemistry, the degree of hydrophilicity will be influenced by nanostructures. On a hydrophilic surface, the presence of nanostructures will lead to increased hydrophilicity (23). This is exemplified by the lower water contact angle for the nanostructured gold surface, as compared with the smooth ones. Hydrophobic bacteria, like *S.*

epidermidis are known to detach more easily and form less biofilm on a hydrophilic surface (27-29). We therefore suggest that the the increased hydrophilicity induced by nanotopography, is a factor contributing to the lower amounts of live bacteria seen on the nanostructured surfaces in our experiments. Furthermore, a small decrease in live bacteria was found when increasing the density of nanoparticles from 17 to 28%, in agreement with a previous study on titanium substrates where an increased surface nanoroughness was shown to decrease bacterial adhesion (17).

We do not exclude that effects apart from nanotopography may have influenced the differences in bacterial behavior on the smooth and nanostructured gold surfaces. In the *in vivo* environment, protein adsorption is a crucial step in both eukaryotic and prokaryotic cell attachment/adhesion (30, 31). The impact of surface chemical properties such as hydrophilicity and surface charge, and of nanotopography on protein adsorption is commonly acknowledged and are known determinants of the proteins that adsorb to a surface and in which manner (32-34). However, in the present study *S. epidermidis* was cultured in protein free RPMI medium on the different experimental surfaces to exclusively study the impact of surface nanotopography on bacterial adhesion.

Overall, higher tower formations and thicker biofilms were found on the smooth surfaces than on nanostructured as seen by scanning electron and confocal microscopy. In addition, the fact that greater surface area was covered by both live and dead bacterial cells on AuNP surfaces indicate that bacteria spread more in the horizontal plane on the AuNP surfaces, and in the vertical plane on smooth surfaces (thicker biofilms).

The initial adhesion events are important since it is when the direct effects of the surface are more evident and restrictions from nutrients and oxygen are usually not an issue. The CLSM observation that a significantly greater area of the AuNP surface interface was covered by

dead cells suggests some type of bactericidal effect upon direct contact with the gold nanotopography. In support, the initial adhesion (2 h) of *S. epidermidis* to nano and smooth surfaces also resulted in a significantly larger dead biomass (429% higher) at the nano surface when compared to dead biomass on smooth surface. In contrast, there was a tendency towards more live biomass on the smooth surfaces. To the best of our knowledge, this is the first report of a bactericidal effect induced solely by nanoparticles immobilized on a surface, since gold is not bactericidal per se (35).

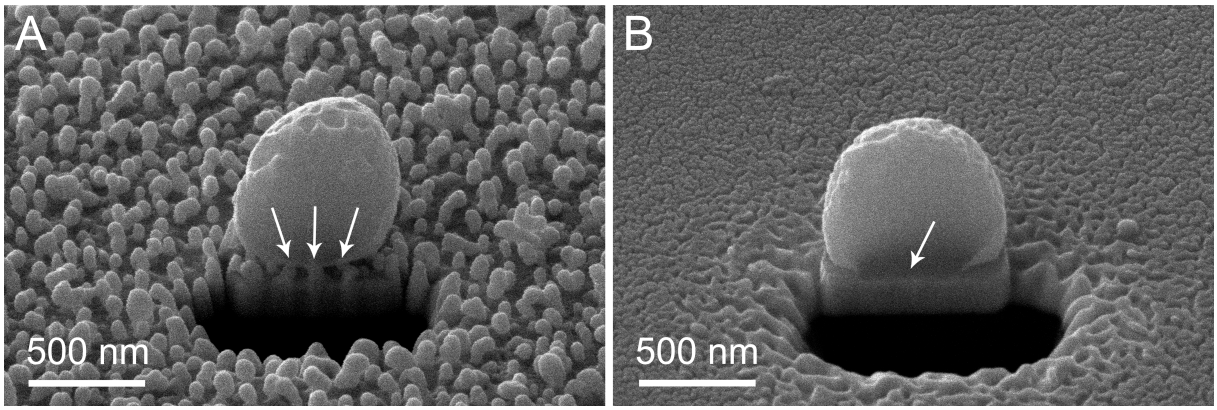

Figure 15. Bacteria-surface interface on AuNP and Au as visualized after ion milling in a FIB-SEM.
The attachment of *Staphylococcus epidermidis* to AuNP relies on a few, discrete attachment points between the bacterial cell wall and the immobilized nanoparticles (arrows in A), while the cell wall is in continuous contact with the smooth surface (arrow in B).

We consider one important factor to be the smaller contact area between the rigid cell wall of the bacteria and the surface, as verified by FIB slice and view, resulting in fewer sites available for adhesion receptor-ligand connections on nanostructured surfaces. Figure 15. This may in turn lead to a different microenvironment that is formed in the confined volume under the bacterial cells and in between the nanoparticles, resulting in e.g. accumulation of waste products, change of pH, and limited flow of nutrients due to formation of a stagnant layer at the interface. Release of nanoparticles from the surface is highly unlikely to be the explanation for the lost bacterial viability due to the firm attachment to the substrate; in fact the nanoparticles are partly sintered to the underlying gold substrate, as seen in Hulander et al

(36). In addition, no visible signs of nanoparticle loss were seen in SEM when comparing the surfaces before and after culture. Based on these observations, a major question is if nanoparticles immobilized on a surface may directly interact with the bacterial cell wall and induce cell death. At present, such assumption has not been verified. The vertical dimension and aspect ratio of the present, immobilized particles may be too small in order to fulfil such mechanism. On the other hand, gold nanoparticles in suspension have shown bactericidal effects in some studies. Cui Y *et al*. studied the molecular mechanism of action of bactericidal NPs on Gram-negative bacteria and demonstrated that Au nanoparticles target energy metabolism and transcription of bacteria by collapse of the membrane potential, resulting in decreased ATP levels and inhibition of the ribosomal subunit from binding tRNA (37).

Differential cell adhesion on gold versus plastic upon microbial stimulation

Different adhesion patterns of the monocytes/macrophages were seen on Au and AuNP compared to TCP: stimulation with zymosan and *S. epidermidis* induced a loss of adherent cells on Au and AuNP, despite the fact that AuNP presented a more hydrophilic substrate for cells. One hypothesis is that this is related to the Au chemistry and its impact on the subsequent protein adsorption that occurs on all surfaces prior to cell attachment. Albeit speculative, an explanation can be the use of different adhesion receptors on Au versus polystyrene (TCP). For example, some receptors are used for both adhesion and phagocytosis(38), and if these events coincide it may result in a detachment from the surface. Previous *in vitro* studies have demonstrated an important role of integrin β2 receptors for the adhesion to material surfaces, NF-κB transcription factor activation and IL-1β, IL-8, MIP-1α and MIP-1β expression (39-42). Additionally, *in vivo* studies have revealed a significantly higher expression of integrin β2 in cells adherent to an implant surface with combined micro- and nano-scale surface texture than a relatively smooth surface (43). The present results show that the integrin β2 gene expression in adherent cells decreased markedly after stimulation

with zymosan and *S. epidermidis*, suggesting a relationship between reduced integrin expression and loss of adherence. On the other hand, a reduced integrin β2 expression after stimulation with the different preys was also observed for the polymer substrates, suggesting that the interaction between Au and monocytes involves other integrins and attachment factors than on the polymer substrates. No firm evidence for this assumption was found after analyzing the gene expression of integrin β1, αv and αm in adherent cells. Further studies, using markers for additional integrins along with blocking experiments with antibodies, would therefore be of interest.

Monocyte activation in response to different substrates and microbial stimulation

Next, we analysed the activity of the cells by measuring the luminol-mediated chemiluminescence (detecting both intra- and extracellular ROS) (44) and the gene and protein expression of selected pro- and anti-inflammatory cytokines. PMN and monocytes are among the first cell types that become adherent to the surface of implants after insertion *in vivo*. The oxidative response and secretion of molecules are influenced both by the properties of the material and the component of their microenvironment (45-47). The early involvement of these cells plays an important role for the inflammatory events and the repair and/or regeneration of soft tissues and bone in association with the implant (48, 49). In addition, when these implant-tissue interface cells encounter and interact with live bacteria, components of their cell walls and other molecules, it is of paramount importance that an efficient immune response is elicited. A major observation in this study was that the amount of CL was dependent on both the type of material surface and the stimulus presented to the monocytes. After stimulation with zymosan and *S. epidermidis*, the total ROS production was higher in cells on polystyrene surfaces than on Au and AuNP. On the other hand, both Au and AuNP surfaces caused a more rapid response in cells challenged with zymosan and *S.*

epidermidis, indicating that the material surface properties influence both the speed and magnitude of the mounted oxidative response. As noted for cell adhesion, chemistry seems to have a more important role than nanotopography. Similarly, chemistry also played the most decisive role when examining TiO-surfaces with 110/160 nm hemispherical protrusions with different surface densities/coverage, where most differences in monocyte/macrophage adhesion and cytokine production and secretion were noted between TiO and TCP, while structured vs. smooth TiO did not differ (50).

In the present study, zymosan promoted a higher ROS production than *S. epidermidis*. This is in agreement with Wagner & Bryers who showed that both opsonized zymosan and exogenous LPS were more potent CL inducers in human monocytes than live *S. epidermidis* (51). Serum-opsonized zymosan elicited a higher total CL in macrophages than opsonized *S. epidermidis* and *Pseudomonas aeruginosa*. Further, opsonization of *S. epidermidis* caused a higher oxidative response than non-opsonized *S. epidermidis*, indicating that activation of the cells via complement and Fc receptors play a role. Moreover, the gene expression of both pro- and anti-inflammatory cytokines as well as superoxide dismutase (SOD) was significantly higher in *S. epidermidis* stimulated samples, indicating that the cells are more active when challenged with live opsonized bacteria than with opsonized zymosan.

Possible *S. epidermidis* molecular candidates for eliciting the ROS-production in monocytes stem from the work of Martinez-Martinez et al(52), showing that *S. epidermidis* cell wall peptidoglycan is the crucial CL inducing component in human PMN cells. The mechanism of CL response induced by *S. epidermidis* may involve the toll-like receptor 2 (TLR2) in activation of NF-KB, as demonstrated for peptidoglycan and lipoteichoic acid from Gram-positive bacteria (53).

The live, opsonized *S. epidermidis* efficiently induced a gene expression of pro-inflammatory TNF-α, IL-1β and IL-6 and anti-inflammatory IL-10. This effect, in contrast to that observed

for ROS production, was higher than with opsonized zymosan. Since this effect was observed for cells on all types of material substrates, no specific role of chemistry and/or nanotopography was suggested. An exception was the Thx surface which promoted a higher expression of pro-inflammatory cytokines in unstimulated cells than the other surfaces.

On the protein level, our results demonstrated a significantly increased secretion of TNF-α by cells stimulated by live, opsonized *S. epidermidis*. Again, no specific modulatory effect of substrate properties was noted. In contrast, the secretion of IL-β and IL-6 had not increased after stimulation. However, the 1 h stimulation period could be too short for detecting the secretion of IL-1 and IL-6. Previously, Gram-negative LPS stimulation of human whole blood induced different time patterns of secreted TNF-α and IL-6 proteins, with a somewhat delayed gene expression and protein secretion for IL-6 in comparison with TNF-α (54). Likewise, the storage of precursor IL-1 intracellularly in human monocytes is followed by a continuous release of IL-1β, starting 2 h after synthesis (55). Zymosan stimulation promoted significantly higher secreted levels of IL-10 in monocytes on AuNP, suggesting an anti-inflammatory potential of the nanofeatures. Tentatively, released Au-ions from the surfaces could result in a anti-inflammatory reaction (56), but measurements of Au in the media (data not shown) indicated low but equal levels in Au and AuNP samples, while elevated levels of IL-10 was only seen for AuNP, indicating that the effect is caused by the nanofeatures rather than leaking Au-ions from the surface. Other studies have found lower gene expression of IL-1β and TNF-α on nano-modified TiO-surfaces (rms 4.8) compared to smooth surfaces using a murine macrophage cell line (57), and less TNF-α protein as well as more rounded human monocytes on 20 nm pores compared to 200 nm pores (11), indicating that small surface nanofeatures may have a down-regulatory effect on monocytes/macrophages.

Taken together, the present data shows that under unstimulated conditions, the different chemistries and topographies of the surfaces did not result in major differences in monocyte viability, surface-induced CL, gene expression and secretion of pro- and anti-inflammatory cytokines. On the other hand, a role of both Au and AuNP substrates was detected in specific inflammatory events when exposed to phagocytic preys, i.e. adhesion, rapidity of CL induction and anti-inflammatory IL-10 secretion.

Conclusion

The difference in surface chemistry (Au vs. polystyrene) seems to have larger effect on the monocytes/macrophages than nanotopography, both for adhesion and activity, when comparing unstimulated cells to zymosan and *S. epidermidis* stimulated cells. The response levels of the cells were more determined by the stimuli origin. However, the amount of live *S. epidermidis* was shown to decrease on nanostructured surfaces compared to smooth ones. In addition, direct contact of *S. epidermidis* with the nanostructured surfaces correlated with a loss in bacterial viability. We therefore suggest that the smaller contact area of the bacterial cell wall with the nanostructured surface as well as the increase in hydrophilicity caused by the nanostructures are important factors for the reduced adhesion and biofilm formation on the nanostructured gold surfaces..

Acknowledgement

This Thesis is based entirely on the article *The role of nanostructured gold surfaces on monocyte activation and Staphylococcus epidermidis biofilm formation,* by Sara Svensson, Magnus Forsberg, Mats Hulander, Forugh Vazirisani, Anders Palmquist, Jukka Lausmaa, Peter Thomsen, Margarita Trobos, accepted for publication in the *International Journal of Nanomedicine*.

The author would like to acknowledge all co-authors and co-workers at the Department of Biomaterials. Furthermore, the author would like to acknowledge the Center for Cellular Imaging, University of Gothenburg where the confocal microscopy was performed, and the Electron Microscopy Unit, University of Gothenburg where the SEM was performed.

Photo credit is given to Mats Hulander for the cover page SEM image visualizing *S. epidermidis* on gold nanoparticles.

Financial support was obtained from BIOMATCELL Vinn Excellence Center of Biomaterials and Cell Therapy, supported by VINNOVA and Region Västra Götaland, the Swedish Research Council (grant K2012-52X- 09495-25-3), The Hjalmar Svensson foundation, IngaBritt and Arne Lundberg Foundation and The Adlerbertska foundation.

Abbreviation list

Au	smooth gold surface
AuND	nanostructured gold surface (Nano Dense)
AuNL	nanostructured gold surface (Nano Light)
AuNP	nanostructured gold surface (Nano Particles)
TCP	tissue culture polystyrene
Thx	tissue culture treated Thermanox® plastic cover slips
AFM	atomic force microscopy
BAI	biomaterial-associated infections
CFU	colony forming units
CL	chemiluminescence
CLSM	confocal laser scanning microscopy
HBSS	Hank's Buffered Salt Solution
IL-1β	interleukin 1beta
IL-10	interleukin 10
IL-6	interleukin 6
LDH	lactate dehydrogenase
OD	optical density
PBS	phosphate buffer solution
ROS	reactive oxygen species
SEM	scanning electron microscopy
TNF- α	tumor necrosis factor alfa
TSB	tryptic soy broth

References

1. Darouiche RO. Treatment of infections associated with surgical implants. N Engl J Med. 2004 Apr 1;350(14):1422-9. PubMed PMID: 15070792. Epub 2004/04/09. eng.
2. Kojic EM, Darouiche RO. Candida infections of medical devices. Clin Microbiol Rev. 2004 Apr;17(2):255-67. PubMed PMID: 15084500. eng.
3. Gristina AG. Implant failure and the immuno-incompetent fibro-inflammatory zone. Clin Orthop Relat Res. 1994 Jan(298):106-18. PubMed PMID: 8118964. eng.
4. Campoccia D, Montanaro L, Arciola CR. The significance of infection related to orthopedic devices and issues of antibiotic resistance. Biomaterials. 2006 Apr;27(11):2331-9. PubMed PMID: 16364434. Epub 2005/12/21. eng.
5. Colon G, Ward BC, Webster TJ. Increased osteoblast and decreased Staphylococcus epidermidis functions on nanophase ZnO and TiO2. J Biomed Mater Res A. 2006 Sep 1;78(3):595-604. PubMed PMID: 16752397. Epub 2006/06/06. eng.
6. Dalby MJ, Giannaras D, Riehle MO, Gadegaard N, Affrossman S, Curtis AS. Rapid fibroblast adhesion to 27nm high polymer demixed nano-topography. Biomaterials. 2004 Jan;25(1):77-83. PubMed PMID: 14580911. Epub 2003/10/29. eng.
7. Dalby MJ, McCloy D, Robertson M, Agheli H, Sutherland D, Affrossman S, et al. Osteoprogenitor response to semi-ordered and random nanotopographies. Biomaterials. 2006 May;27(15):2980-7. PubMed PMID: 16443268. Epub 2006/01/31. eng.
8. Kubo K, Tsukimura N, Iwasa F, Ueno T, Saruwatari L, Aita H, et al. Cellular behavior on TiO2 nanonodular structures in a micro-to-nanoscale hierarchy model. Biomaterials. 2009 Oct;30(29):5319-29. PubMed PMID: 19589591. Epub 2009/07/11. eng.
9. Puckett SD, Lee PP, Ciombor DM, Aaron RK, Webster TJ. Nanotextured titanium surfaces for enhancing skin growth on transcutaneous osseointegrated devices. Acta Biomater. 2010 Jun;6(6):2352-62. PubMed PMID: 20005310. Epub 2009/12/17. eng.
10. Smith LL, Niziolek PJ, Haberstroh KM, Nauman EA, Webster TJ. Decreased fibroblast and increased osteoblast adhesion on nanostructured NaOH-etched PLGA scaffolds. Int J Nanomedicine. 2007;2(3):383-8. PubMed PMID: 18019837. Pubmed Central PMCID: 2676656. Epub 2007/11/21. eng.
11. Ferraz N, Hong J, Santin M, Karlsson Ott M. Nanoporosity of alumina surfaces induces different patterns of activation in adhering monocytes/macrophages. Int J Biomater. 2010;2010:402715. PubMed PMID: 21234322. Pubmed Central PMCID: 3018647. Epub 2011/01/15. eng.
12. Mohiuddin M, Pan HA, Hung YC, Huang GS. Control of growth and inflammatory response of macrophages and foam cells with nanotopography. Nanoscale Res Lett. 2012;7(1):394. PubMed PMID: 22799434. Pubmed Central PMCID: 3507756. Epub 2012/07/18. eng.
13. Wojciak-Stothard B, Curtis A, Monaghan W, MacDonald K, Wilkinson C. Guidance and activation of murine macrophages by nanometric scale topography. Exp Cell Res. 1996 Mar 15;223(2):426-35. PubMed PMID: 8601420. Epub 1996/03/15. eng.
14. Anselme K, Davidson P, Popa AM, Giazzon M, Liley M, Ploux L. The interaction of cells and bacteria with surfaces structured at the nanometre scale. Acta Biomater. 2010 Oct;6(10):3824-46. PubMed PMID: 20371386. Epub 2010/04/08. eng.
15. Mitik-Dineva N, Wang J, Truong VK, Stoddart P, Malherbe F, Crawford RJ, et al. Escherichia coli, Pseudomonas aeruginosa, and Staphylococcus aureus attachment patterns on glass surfaces with nanoscale roughness. Curr Microbiol. 2009 Mar;58(3):268-73. PubMed PMID: 19020934. Epub 2008/11/21. eng.

16. Mitik-Dineva N, Wang J, Truong VK, Stoddart PR, Malherbe F, Crawford RJ, et al. Differences in colonisation of five marine bacteria on two types of glass surfaces. Biofouling. 2009 Oct;25(7):621-31. PubMed PMID: 20183121. Epub 2010/02/26. eng.
17. Puckett SD, Taylor E, Raimondo T, Webster TJ. The relationship between the nanostructure of titanium surfaces and bacterial attachment. Biomaterials. 2010 Feb;31(4):706-13. PubMed PMID: 19879645. Epub 2009/11/03. eng.
18. Hulander M, Lundgren A, Berglin M, Ohrlander M, Lausmaa J, Elwing H. Immune complement activation is attenuated by surface nanotopography. Int J Nanomedicine. 2011;6:2653-66. PubMed PMID: 22114496. Pubmed Central PMCID: 3218579. Epub 2011/11/25. eng.
19. Kimling J, Maier M, Okenve B, Kotaidis V, Ballot H, Plech A. Turkevich method for gold nanoparticle synthesis revisited. J Phys Chem B. 2006 Aug 17;110(32):15700-7. PubMed PMID: 16898714. Epub 2006/08/11. eng.
20. Hulander M, Lundgren A, Faxälv L, Lindahl TL, Palmquist A, Berglin M, et al. Gradients in surface nanotopography used to study platelet adhesion and activation. Colloids and Surfaces B: Biointerfaces. 2013 (0).
21. Lundgren AO, Bjoerefors F, Olofsson LGM, Elwing H. Self-Arrangement Among Charge-Stabilized Gold Nanoparticles on a Dithiothreitol Reactivated Octanedithiol Monolayer. Nano Letters. 2008 Nov;8(11):3989-92. PubMed PMID: WOS:000260888600077.
22. Heydorn A, Nielsen AT, Hentzer M, Sternberg C, Givskov M, Ersboll BK, et al. Quantification of biofilm structures by the novel computer program COMSTAT. Microbiology. 2000 Oct;146 (Pt 10):2395-407. PubMed PMID: 11021916. Epub 2000/10/06. eng.
23. Sheng YJ, Jiang S, Tsao HK. Effects of geometrical characteristics of surface roughness on droplet wetting. The Journal of chemical physics. 2007 Dec 21;127(23):234704. PubMed PMID: 18154406. Epub 2007/12/25. eng.
24. Kiener PA, Davis PM, Starling GC, Mehlin C, Klebanoff SJ, Ledbetter JA, et al. Differential induction of apoptosis by Fas-Fas ligand interactions in human monocytes and macrophages. J Exp Med. 1997 Apr 21;185(8):1511-6. PubMed PMID: 9126933. Pubmed Central PMCID: 2196275. Epub 1997/04/21. eng.
25. Ercan B, Taylor E, Alpaslan E, Webster TJ. Diameter of titanium nanotubes influences anti-bacterial efficacy. Nanotechnology. 2011 Jul 22;22(29):295102. PubMed PMID: 21673387. Epub 2011/06/16. eng.
26. Machado MC, Tarquinio KM, Webster TJ. Decreased Staphylococcus aureus biofilm formation on nanomodified endotracheal tubes: a dynamic airway model. Int J Nanomedicine. 2012;7:3741-50. PubMed PMID: 22904622. Pubmed Central PMCID: 3418105. Epub 2012/08/21. eng.
27. An YH, Friedman RJ. Concise review of mechanisms of bacterial adhesion to biomaterial surfaces. J Biomed Mater Res. 1998 Fall;43(3):338-48. PubMed PMID: 9730073. Epub 1998/09/08. eng.
28. Boks NP, Norde W, van der Mei HC, Busscher HJ. Forces involved in bacterial adhesion to hydrophilic and hydrophobic surfaces. Microbiology. 2008 Oct;154(Pt 10):3122-33. PubMed PMID: 18832318. Epub 2008/10/04. eng.
29. Braem A, Van Mellaert L, Mattheys T, Hofmans D, De Waelheyns E, Geris L, et al. Staphylococcal biofilm growth on smooth and porous titanium coatings for biomedical applications. J Biomed Mater Res A. 2013 May 10. PubMed PMID: 23661274. Epub 2013/05/11. Eng.
30. Nilsdotter-Augustinsson A, Claesson C, Lindgren PE, Lundqvist-Gustafsson H, Ohman L. Adherence of Staphylococcus epidermidis to extracellular matrix proteins and

effects of fibrinogen-bound bacteria on oxidase activity and apoptosis in neutrophils. APMIS. 2005 May;113(5):361-73. PubMed PMID: 16011663. Epub 2005/07/14. eng.
31. Wilson CJ, Clegg RE, Leavesley DI, Pearcy MJ. Mediation of biomaterial-cell interactions by adsorbed proteins: a review. Tissue Eng. 2005 Jan-Feb;11(1-2):1-18. PubMed PMID: 15738657. Epub 2005/03/02. eng.
32. Roach P, Farrar D, Perry CC. Surface tailoring for controlled protein adsorption: effect of topography at the nanometer scale and chemistry. J Am Chem Soc. 2006 Mar 29;128(12):3939-45. PubMed PMID: 16551101. Epub 2006/03/23. eng.
33. Steiner G, Tunc S, Maitz M, Salzer R. Conformational changes during protein adsorption. FT-IR spectroscopic imaging of adsorbed fibrinogen layers. Anal Chem. 2007 Feb 15;79(4):1311-6. PubMed PMID: 17297929. Epub 2007/02/15. eng.
34. Xu LC, Siedlecki CA. Effects of surface wettability and contact time on protein adhesion to biomaterial surfaces. Biomaterials. 2007 Aug;28(22):3273-83. PubMed PMID: 17466368. Pubmed Central PMCID: 3671914. Epub 2007/05/01. eng.
35. Tran N, Tran PA. Nanomaterial-based treatments for medical device-associated infections. Chemphyschem : a European journal of chemical physics and physical chemistry. 2012 Jul 16;13(10):2481-94. PubMed PMID: 22517627. Epub 2012/04/21. eng.
36. Hulander M, Lundgren A, Faxalv L, Lindahl TL, Palmquist A, Berglin M, et al. Gradients in surface nanotopography used to study platelet adhesion and activation. Colloids Surf B Biointerfaces. 2013 Oct 1;110:261-9. PubMed PMID: 23732803. Epub 2013/06/05. eng.
37. Cui Y, Zhao Y, Tian Y, Zhang W, Lu X, Jiang X. The molecular mechanism of action of bactericidal gold nanoparticles on Escherichia coli. Biomaterials. 2012 Mar;33(7):2327-33. PubMed PMID: 22182745. Epub 2011/12/21. eng.
38. Aderem A, Underhill DM. Mechanisms of phagocytosis in macrophages. Annu Rev Immunol. 1999;17:593-623. PubMed PMID: 10358769. Epub 1999/06/08. eng.
39. Collie AM, Bota PC, Johns RE, Maier RV, Stayton PS. Differential monocyte/macrophage interleukin-1beta production due to biomaterial topography requires the beta2 integrin signaling pathway. J Biomed Mater Res A. 2011 Jan;96(1):162-9. PubMed PMID: 21105164. Epub 2010/11/26. eng.
40. Perez RL, Roman J. Fibrin enhances the expression of IL-1 beta by human peripheral blood mononuclear cells. Implications in pulmonary inflammation. J Immunol. 1995 Feb 15;154(4):1879-87. PubMed PMID: 7836771. Epub 1995/02/15. eng.
41. Rezzonico R, Chicheportiche R, Imbert V, Dayer JM. Engagement of CD11b and CD11c beta2 integrin by antibodies or soluble CD23 induces IL-1beta production on primary human monocytes through mitogen-activated protein kinase-dependent pathways. Blood. 2000 Jun 15;95(12):3868-77. PubMed PMID: 10845922. Epub 2000/06/14. eng.
42. Rezzonico R, Imbert V, Chicheportiche R, Dayer JM. Ligation of CD11b and CD11c beta(2) integrins by antibodies or soluble CD23 induces macrophage inflammatory protein 1alpha (MIP-1alpha) and MIP-1beta production in primary human monocytes through a pathway dependent on nuclear factor-kappaB. Blood. 2001 May 15;97(10):2932-40. PubMed PMID: 11342414. Epub 2001/05/09. eng.
43. Omar O, Lenneras M, Svensson S, Suska F, Emanuelsson L, Hall J, et al. Integrin and chemokine receptor gene expression in implant-adherent cells during early osseointegration. J Mater Sci Mater Med. 2010 Mar;21(3):969-80. PubMed PMID: 19856201. Epub 2009/10/27. eng.
44. Jancinova V, Drabikova K, Nosal R, Rackova L, Majekova M, Holomanova D. The combined luminol/isoluminol chemiluminescence method for differentiating between extracellular and intracellular oxidant production by neutrophils. Redox Rep. 2006;11(3):110-6. PubMed PMID: 16805965. Epub 2006/06/30. eng.

45. Lindblad M, Lestelius M, Johansson A, Tengvall P, Thomsen P. Cell and soft tissue interactions with methyl- and hydroxyl-terminated alkane thiols on gold surfaces. Biomaterials. 1997 Aug;18(15):1059-68. PubMed PMID: 9239468. Epub 1997/08/01. eng.
46. Suska F, Gretzer C, Esposito M, Emanuelsson L, Wennerberg A, Tengvall P, et al. In vivo cytokine secretion and NF-kappaB activation around titanium and copper implants. Biomaterials. 2005 Feb;26(5):519-27. PubMed PMID: 15276360. Pubmed Central PMCID: 1. eng.
47. Suska F, Svensson S, Johansson A, Emanuelsson L, Karlholm H, Ohrlander M, et al. In vivo evaluation of noble metal coatings. J Biomed Mater Res B Appl Biomater. 2010 Jan;92(1):86-94. PubMed PMID: 19701914. Epub 2009/08/25. eng.
48. Omar OM, Lenneras ME, Suska F, Emanuelsson L, Hall JM, Palmquist A, et al. The correlation between gene expression of proinflammatory markers and bone formation during osseointegration with titanium implants. Biomaterials. 2011 Jan;32(2):374-86. PubMed PMID: 20933278. Epub 2010/10/12. eng.
49. Suska F, Emanuelsson L, Johansson A, Tengvall P, Thomsen P. Fibrous capsule formation around titanium and copper. J Biomed Mater Res A. 2008 Jun 15;85(4):888-96. PubMed PMID: 17896778. Epub 2007/09/28. eng.
50. Rice JM, Hunt JA, Gallagher JA, Hanarp P, Sutherland DS, Gold J. Quantitative assessment of the response of primary derived human osteoblasts and macrophages to a range of nanotopography surfaces in a single culture model in vitro. Biomaterials. 2003 Nov;24(26):4799-818. PubMed PMID: 14530077. Epub 2003/10/08. eng.
51. Wagner VE, Bryers JD. Poly(ethylene glycol)-polyacrylate copolymers modified to control adherent monocyte-macrophage physiology: interactions with attaching Staphylococcus epidermidis or Pseudomonas aeruginosa bacteria. J Biomed Mater Res A. 2004 Apr 1;69(1):79-90. PubMed PMID: 14999754. Epub 2004/03/05. eng.
52. Martinez-Martinez L, Timmerman CP, Fleer A, Verhoef J. Chemiluminescence of human polymorphonuclear leucocytes after stimulation with whole cells and cell-wall components of Staphylococcus epidermidis. J Med Microbiol. 1993 Sep;39(3):196-203. PubMed PMID: 8366518. Epub 1993/09/01. eng.
53. Schwandner R, Dziarski R, Wesche H, Rothe M, Kirschning CJ. Peptidoglycan- and lipoteichoic acid-induced cell activation is mediated by toll-like receptor 2. J Biol Chem. 1999 Jun 18;274(25):17406-9. PubMed PMID: 10364168. Epub 1999/06/11. eng.
54. DeForge LE, Remick DG. Kinetics of TNF, IL-6, and IL-8 gene expression in LPS-stimulated human whole blood. Biochem Biophys Res Commun. 1991 Jan 15;174(1):18-24. PubMed PMID: 1989598. Epub 1991/01/15. eng.
55. Hazuda DJ, Lee JC, Young PR. The kinetics of interleukin 1 secretion from activated monocytes. Differences between interleukin 1 alpha and interleukin 1 beta. J Biol Chem. 1988 Jun 15;263(17):8473-9. PubMed PMID: 3259579. Epub 1988/06/15. eng.
56. Eisler R. Chrysotherapy: a synoptic review. Inflamm Res. 2003 Dec;52(12):487-501. PubMed PMID: 14991077. Pubmed Central PMCID: 1. eng.
57. Lee S, Choi J, Shin S, Im YM, Song J, Kang SS, et al. Analysis on migration and activation of live macrophages on transparent flat and nanostructured titanium. Acta Biomater. 2011 May;7(5):2337-44. PubMed PMID: 21232636. Epub 2011/01/15. eng.

Populärvetenskaplig sammanfattning

I dagens samhälle med en allt större aktiv åldrande befolkning samt en sjukvård som kan erbjuda allt fler avancerade ingrepp ställs allt större krav på densamma. Operationer såsom exempelvis höftledsproteser, knäproteser och tandimplantat blir allt vanligare. Proteser, implantat och katetrar är för kroppen främmande material som i den bästa av världar skall vara lämpade för ändamålet i form av funktion och hållfasthet men även lika viktigt är att de skall vara kompatibla till kroppens vävnader, de skall vara biomaterial.

Den generellt sett mest fruktade komplikationen till användandet av biomaterial är en infektion. Det beror på att infektioner i anslutning till biomaterial är mycket problematiska för patienten, hälso- och sjukvården samt samhället i stort. Konsekvenserna av en sådan infektion kan vara förödande, bl.a. i regel ett behov av att avlägsna implantatet men även livshotande systemiska infektioner kan uppkomma.

Under normala förhållanden kommer bakterier och andra mikroorganismer som kommer in i kroppen hållas under kontroll av immunsystemet. Den första linjen av vårt immunförsvar innefattar en mängd faktorer, ex. barriärer såsom vår egen hud och slemhinnor, proteiner som dödar bakterier samt signalsubstanser som aktiverar våra försvarsceller, de vita blodkropparna. När ett främmande material, tex en höftprotes eller urinkateter, är närvarande försvåras vårt försvar bland annat genom att bakterier kan fastna på ytan av materialet och bilda en så kallad biofilm vilken består av bakterier tillsammans med slime som bakterierna har producerat.

Denna biofilm skyddar bakterierna från de vita blodkropparna samt mot antibakteriella antikroppar som kroppen kan bilda såväl som mot antibiotika som får betydligt svårare att avdöda bakterierna. Dessa orsaker i kombination med att fler bakterier utvecklar resistens mot antibiotika är viktiga skäl för förebyggande åtgärder i syfte att minska infektioner vid användandet av biomaterial.

Vår egen huds normalflora som består av arter ur den gram-positiva familjen *Staphylococcus*, särskilt *Staphylococcus epidermidis* och *Staphylococcus aureus* är de dominerande arterna i infektioner på biomaterial och står för ca 66 % av dessa infektioner.

Material med nanotopografi har tidigare undersökts med avseende på vidhäftning och funktionen hos olika celltyper, t.ex. bindvävsskapande celler (fibroblaster) och benskapande celler (osteoblaster) och nanostrukturerade material har också föreslagits spela en roll i bakteriell vidhäftning. En nanometer (nm) är en miljarddels meter vilket är en oerhört liten enhet. Som jämförelse är ett hårstrå som vi har på huvudet ca 60 mikrometer i diameter vilket innebär att det är 60 000 nm brett samt att en bakterie av typen *S. epidermidis* är ca 500 nm stor.

I denna studie har vi undersökt huruvida nanostrukturer har en effekt på bakteriell vidhäftning och bildning av biofilm och/eller har en inverkan på beteendet hos immunceller som svar på mikrobiella stimuli. För detta ändamål har vi valt att använda guldtäckta kiseldioxidplattor (8x8mm) på vilka vi har fäst guldnanopartiklar som har varit 35-40 nm stora. Som kontroll har vi dels använt släta guldytor, dels två olika plastytor för att se vilken eventuell inverkan som guldytan i sig själv har på bakterierna.

Resultaten i studien visar att skillnaden i ytornas kemi (guld i jämförelse med plast) verkar ha större effekt på kroppens försvarsceller, monocyterna än vad nanotopografin har, både för vidhäftning och aktivitet, detta när man jämför ostimulerade celler med celler som har blivit stimulerade av bakterier. Emellertid var mängden levande *S. epidermidis* minskad på nanostrukturerade guldytor jämfört med släta guldytor. Dessutom när *S. epidermidis* kom i direkt kontakt med de nanostrukturerade ytorna visade det på en förlust i bakteriell

livsduglighet. Våra data visar att bakteriell vidhäftning på nanostrukturerade hydrofila ytor är nära förbunden med den ökade ytenergin (ökad hydrofilicitet) vilken orsakas av förekomsten av nanostrukturer, vilket i sin tur resulterar i bakteriedöd och minskad vidhäftning.

Biomaterial för att användas i olika typer av implantat är en viktig del i sjukvårdens möjligheter för att kunna erbjuda såväl gamla som unga goda möjligheter till ett aktivt och hälsosamt liv. Samhället i stort behöver samtidigt vara mer restriktivt vid förskrivning av antibiotika för att vi i framtiden skall kunna erbjuda en säker sjukvård med stora möjligheter till bot.

Forskning inom området är därför mycket viktig för utvecklingen av nya säkra biomaterial och våra resultat visar att nanotopografi kan inhibera bakterietillväxt och därmed kan vara en möjlig väg att gå för at få färre implantat-relaterade infektioner. Slutligen behöver det forskas mer på olika material och ytskikt innan vi når fram till att nya material kan användas inom den kliniska vardagen men förutsättningarna ser ut att finnas för att möta de utmaningar som står oss till mötes.